Crystallization, Melting Behavior, Physical Properties, and Physical Aging of Ethylene/1-Octene Copolymers

Sha Yang

Thesis submitted to the faculty of the Virginia Polytechnic Institute and State University in partial fulfillment of the requirements for the degree of

Master of Science

in

Chemistry

Hervé Marand, Committee Chair

Alan R. Esker

Garth L. Wilkes

May 3, 2011

Blacksburg, VA

Keywords: ethylene/1-octene copolymers, melting, crystallization, physical aging

Crystallization, Melting Behavior, Physical Properties, and Physical Aging of Ethylene/1-Octene Copolymers

Sha Yang

Abstract

The time dependence of the physical properties of ethylene/1-octene (EO)-copolymers after primary crystallization is investigated by calorimetry, density, and creep measurements.

The temporal evolution of the multiple melting of EO-copolymers is monitored by differential scanning calorimetry. The low temperature endotherm displays an evolution similar to that observed for the enthalpy recovery in glasses after physical aging. Using this analogy, a calorimetry-aging rate is defined, which quantifies the change in the low endotherm temperature with time. Similarly a density-aging rate is defined from the evolution of density with time.

A non-classical creep behavior is observed for short aging times, consistent with crystallization-induced shrinkage. The change in crystallinity during aging leads to a change in the shape of the relaxation spectrum. Hence, analysis of creep data cannot be carried out using Struik's superposition method. For both short and long aging times, the creep rate exhibits a dependence on copolymer composition similar to those associated with the calorimetry- and the density-aging rates, suggesting a common origin for the evolution of the low endotherm, the creep behavior and the bulk density.

The calorimetry, density, and creep data are reexamined based on the following assumptions:

First, a single population of small crystals is formed during crystallization at low temperature; Second, these small crystals increase in stability under isothermal conditions, easily melt and recrystallize during heating and serve as efficient thermo-reversible cross-links to increase the conformational constraints in the residual amorphous fraction. These assumptions appear to be consistent with all observations made to date.

Acknowledgements

I would like to express my sincere appreciation to my advisor, Dr. Hervé Marand, for his help and invaluable guidance.

I would like to thank Dr. Alan R. Esker, Dr. Garth L. Wilkes and Dr. Paul Deck for serving on my committee and for their useful remarks on my thesis.

I would like to thank Peter Caulfield for RHC DSC training.

Thanks to Dow Chemical and TA Instruments for providing the materials and equipments for this research project.

Finally, I wish to express my deepest appreciation to my family and friends who provided encouragement throughout my study.

Table of Contents

List of Figures

List of Tables

Chapter 1. Introduction

The goal of this research project is to understand the origin of the time dependence of the structure and physical properties of ethylene/1-octene (EO)-copolymers, and the possible correlations between physical aging, secondary crystallization, and melting-recrystallization-remelting. Three different types of experimental techniques are used, namely, differential scanning calorimetry (DSC), density, and creep.

Chapter 2 introduces the background of bulk crystallization (primary and secondary crystallization); melting of semicrystalline polymers and copolymers, morphology of EO-copolymers; and physical aging. Chapter 3 provides the experimental details associated with these investigations, including the material characteristics (octene content, weight average molecular weight (M_w), polydispersity index (PDI) and density) and the conditions under which experimental techniques (DSC, density, and creep) were utilized. Chapter 4 gives the results of these measurements and the discussion of the time dependent physical properties. Chapter 5 provides conclusions and suggests future studies.

Chapter 2. Background

2.1 Crystallization

Bulk crystallization occurs in two stages: primary crystallization and secondary crystallization. This review first focuses on flexible chain homopolymers without structural or compositional defects and only considers quiescent crystallization (no orientation) from the melt, because such materials rarely exhibit multiple-melting behavior. The special case of copolymers is dealt with subsequently.

2.1.1 Primary Crystallization

Primary crystallization is the process associated with the formation of semicrystalline superstructures (hedrites, axialites, and, most frequently, spherulites). The growth stages associated with primary crystallization are illustrated in Figure 2.1, for a polymer spherulite consisting of chain-folded lamellar crystals: 1) a primary nucleus leads to the formation of a single crystal; 2) a multiple layer crystal results from screw dislocations; 3) repeated branching and splaying of lamellae leads to an axialite, then, to a sheaf-like structure, and finally to a spherulite.[1] The end of the primary crystallization stage is marked by the impingement of neighboring spherulites initiated by different nuclei.

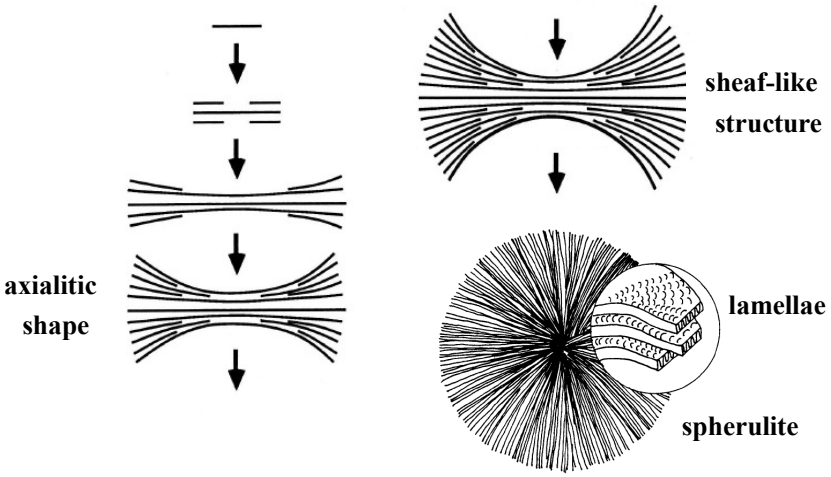

Figure 2.1. Growth stages of a polymer spherulite with chain-folded lamellae (adapted from reference 1).

2.1.1.1 Observations for Primary Crystallization

The growth rate of polymer crystals is constant under isothermal conditions but varies with the crystallization temperature. As illustrated in Figure 2.2 for isotactic polystyrene (it-PS), the growth rate exhibits a bell-shaped curve and approaches zero when the crystallization temperature approaches either the polymer's glass transition temperature (ca. 100 °C) or its melting temperature (ca. 260 °C).[2]

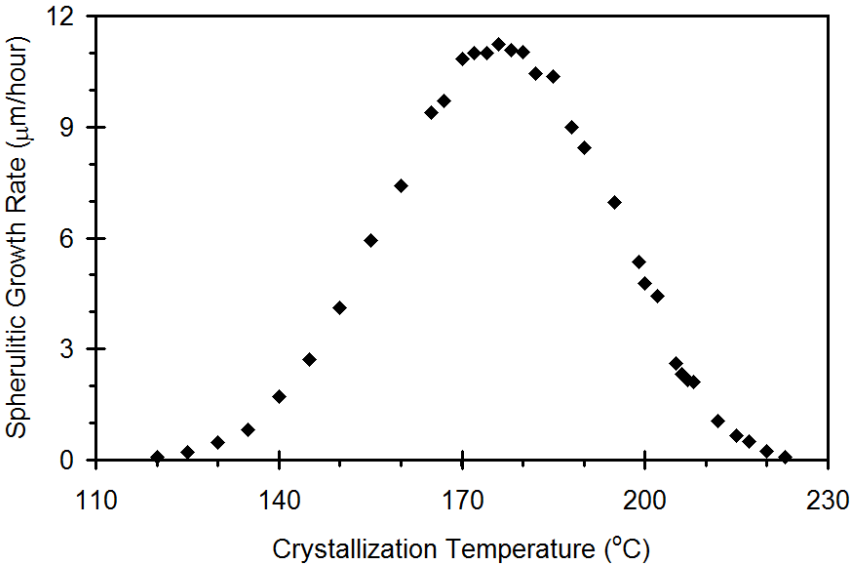

Figure 2.2. Spherulitic growth rate vs. crystallization temperature for isotactic polystyrene (adapted from reference 2).

Another general observation is that lamellar crystals are thin chain-folded plate-like structures, where the thin dimension is along the chain axis and the basal crystal planes contain the chain folds. The average thickness of lamellae increases with crystallization temperature, more significantly so, when crystallization occurs at lower undercooling (Figure 2.3).[3] Lamellar crystals are sometimes observed to thicken with increasing crystallization time (Figure 2.4).[4] This thickening process is driven by the increase in crystal stability associated with the decrease in the crystal surface area to volume ratio.

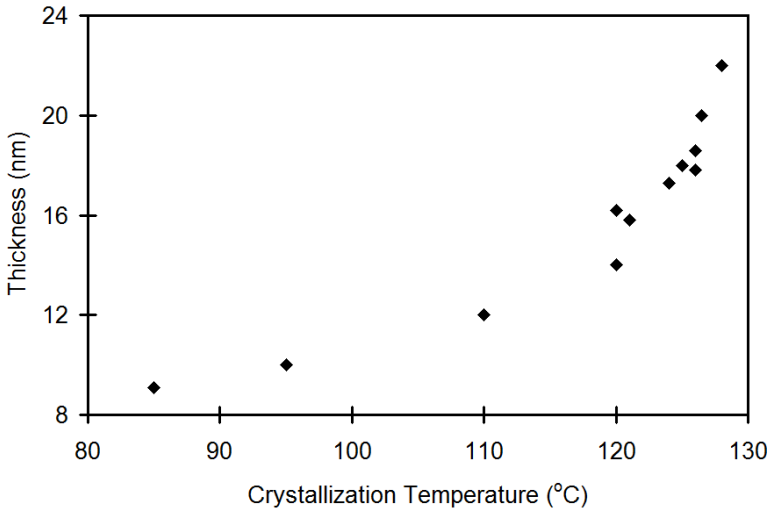

Figure 2.3. Lamellar thickness as a function of crystallization temperature for polyethylene (adapted from reference 3).

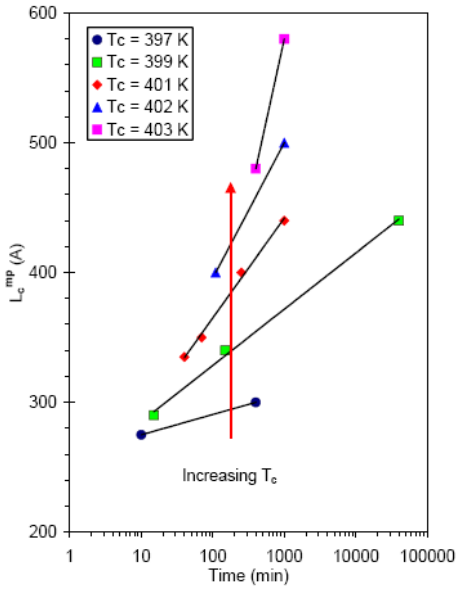

Figure 2.4. Lamellar thickness as a function of crystallization time for polyethylene (adapted from reference 4).

2.1.1.2 Melting Behavior of Polymer Crystals

The melting temperature is one of the most important thermodynamic properties of a crystallizable polymer. The melting temperature observed experimentally depends on the conditions under which the polymer is crystallized. Several models have been proposed to evaluate the equilibrium or thermodynamic melting point, T_m. The Hoffman-Weeks analysis,[5] which is based on predictions from the Lauritzen-Hoffman kinetic theory[6] of crystallization, proposes a linear relationship between observed melting temperature, T_m', and crystallization temperature, T_x, at relatively small undercooling:

$$T_m' = T_m\left(1-\frac{1}{\gamma}\right)+\frac{1}{\gamma}T_x \tag{2.1}$$

where γ is the coefficient of thickening of the lamellae. The equilibrium melting temperature is determined in a T_m' vs. T_x plot from the intercept of the extrapolated linear relationship between T_m' and T_x with the line $T_m' = T_x$ (Figure 2.5).

Application of the linear Hoffman-Weeks treatment is limited because it neglects a term, which accounts for the lamellar thickness increment and the temperature dependence of the fold surface free energy.[7] By re-examining the various assumptions inherent to the Hoffman-Weeks approach, Marand's group[7] has proposed a nonlinear approach for a more accurate estimation of equilibrium melting temperatures (Figure 2.5).

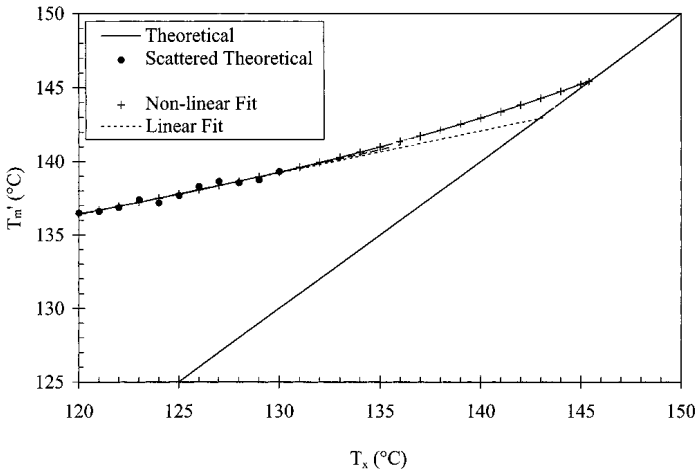

Figure 2.5. Linear Hoffman-Week extrapolation and nonlinear fit.[7]

Recently, in a significant departure from conventional wisdom, Strobl and coworkers[8-14] proposed that crystallization occurs from a mesomorphic phase rather than from the isotropic phase and defined different thermodynamic temperatures for crystallization (mesomorphic to crystal) and melting (crystal to isotropic melt). On the basis of time- and temperature-dependent small angle X-ray scattering (SAXS) measurements, they suggest that the equilibrium crystallization temperature is always higher than the equilibrium melting temperature.[12] They also suggest that the equilibrium melting and crystallization temperatures are both higher than the zero growth temperature, which is the temperature controlling the growth rate of polymer crystals. The zero growth temperature is the temperature associated with the equilibrium between the isotropic and the mesomorphic phases.

2.1.1.3 Abbreviated Kinetic Theory of Polymer Crystallization

Observation of linear growth (crystal growth rate is independent of time) and of a strong temperature dependence of crystallization rates have led to suggestions that polymer crystal growth is controlled by secondary nucleation.[6] In this context, the rate of crystal growth is a function of the driving force for crystallization and the barrier to secondary nucleation.

The Lauritzen-Hoffman (LH) theory is one of the main kinetic theories of polymer crystallization.[6, 15-18] According to the LH theory, the free energy change for the formation of a lamellar crystal at T_x, $\Delta G_c(T_x)$, can be used to describe the driving force quantitatively.

If we denote X and Y as the lateral crystal dimensions, l as the crystal thickness, σ as the lateral surface free energy, and σ_e as the fold surface free energy, we can express $\Delta G_c(T_x)$ as follows for the crystal shown in Figure 2.6 after neglecting the small σ-containing term:

$$\Delta G_c(T) = 2\sigma_e XY(1 - l/l_{min}) \qquad (2.2)$$

where $l_{min} = 2\sigma_e / \Delta G_f^0(T_x)$, which is the minimum possible crystal thickness at the crystallization temperature, T_x. In equation 2.2, $\Delta G_f^0(T_x)$ is the bulk free energy of fusion per unit volume of crystal at the crystallization temperature. This quantity is well approximated by $\Delta G_f^0(T_x) \sim \Delta H_f^0(T_x)\,(T_m - T_x)/T_m$, where ΔH_f^0 is the bulk heat of fusion of the polymer crystal per unit volume.

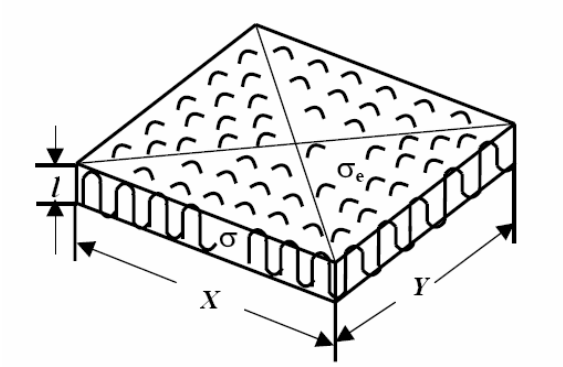

Figure 2.6. Schematic of a chain-folded lamellar single crystal (adapted from reference 15).

The larger the lamellar thickness, the larger the free energy change during crystallization, the larger the driving force. On the other hand, the free energy barrier for nucleation increases with lamellar thickness. The rate of crystallization is the result of the interplay between the free energy barrier for nucleation and the driving force. The LH nucleation theory assumes that crystal growth occurs by a chain folding mechanism. The two-step kinetically controlled mechanism (Figure 2.7) consists in the deposition of an initial stem on a clean surface (nucleation), and the subsequent and repeated folding of the rest of the chain to complete the layer (substrate completion). As both the driving force for crystallization and the barrier to nucleation increase with the lamellar thickness, l, an optimum lamellar thickness is required to maximize the growth rate at each crystallization temperature.

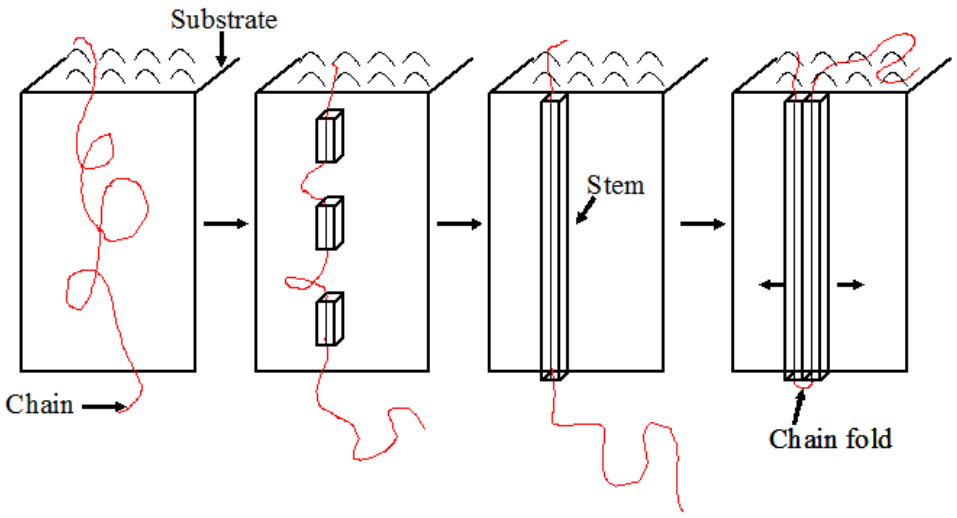

Figure 2.7. Schematic describing the secondary nucleation and the substrate completion processes (adapted from reference 6).

Strobl[11, 14] proposed another model for polymer crystallization, which suggests that the formation and growth of the crystallites is a multi-step process involving the formation of a mesomorphic layer by attachment of chains onto the growth front. The mesomorphic layer thickens with time as the mobility of chains within this phase is high. Solidification occurs by a structural transition when the mesomorphic layer reaches a critical thickness. A "granular crystal or block" is used to describe the resulting structure. The last step is the increase in internal perfection by merging the blocks together. This model is proposed based on the experiments carried out by Strobl et al.[11, 14] (SAXS and DSC experiments), Kanig et al.[19] (observation of mesomorphic layers prior to the formation of the PE lamellar crystallites by transmission electron microscopy), Rastogi et al.[20] (observation by optical microscopy of a two step process during the formation of PE crystallites under high pressure), and Okada et al.[21] (observation by

light scattering of density fluctuations in the melt prior to the appearance of the first crystallites in the case of it-PP). Figure 2.8 provides a snapshot of the transformation of the melt into the final lamellar crystallite.

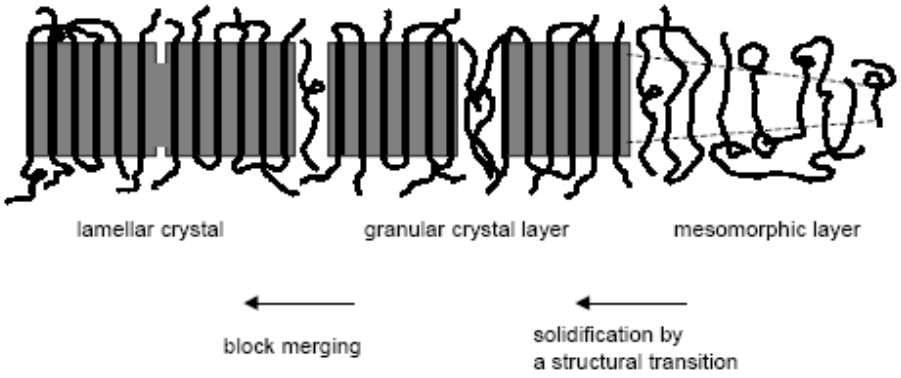

Figure 2.8. Sketch of the different stages in the formation of polymer crystallites according to Strobl et al. [11]

The differences between the LH and the Strobl models are: 1) the LH model considers only two phases (liquid phase and crystalline phase) while the Strobl model also considers an intermediate mesomorphic phase; 2) the LH model assumes a chain folding process, where the chains attach to the growth front in a crystallographic fashion, whereas the Strobl model assumes neither chain folding nor crystallographic registration during the first stage. Hence, the undercooling below the melt to mesomorphic transition controls the crystal growth rate.

2.1.1.4 Crystallinity

Crystallization is a function of thermodynamics and kinetics. Sections of polymer chains that are rejected or trapped between crystal lamellae during crystallization will generate an amorphous phase. As crystallization is never complete, a degree of crystallinity is introduced and denoted by X_c (also referred to as "crystallinity index", or "percent crystallinity"). When crystallinity is expressed as the fraction of the total mass exhibiting crystalline order, we can write:

$$X_c = \frac{m_c}{m_a + m_c} \tag{2.3}$$

where m_c is the mass of the crystalline phase and m_a is the mass of the amorphous phase. Using this definition, any intensive property P of a semicrystalline polymer can be represented by a weighted average of the "partial properties" of the crystalline and the amorphous components-P_c and P_a[22]

$$P = X_c P_c + X_a P_a \tag{2.4}$$

where $X_a = 1 - X_c$. Equation 2.4 corresponds to the 2-phase model of semicrystalline polymers.

2.1.2 Secondary Crystallization

It has been widely reported[23-26] that many physical properties of semicrystalline polymers, such as the density or the modulus, still increase after primary crystallization, as a result of a further increase in crystallinity. The term “secondary crystallization” is used to describe the

increase in the degree of crystallinity with time after the growth and impingement of spherulites.

On the basis of calorimetric studies of the melting behavior of semicrystalline polymers, one can distinguish two classes of secondary crystallization processes. In the case of high crystallinity flexible polymers, such as poly(ethylene oxide) (PEO) and linear polyethylene (PE), the melting behavior is characterized by a single melting endotherm (Figure 2.9).[5, 27-29] Secondary crystallization is only observed at high temperature close to the melting point (undercooling of 20 K for PEO). The crystallinity increases slowly over decades of time.

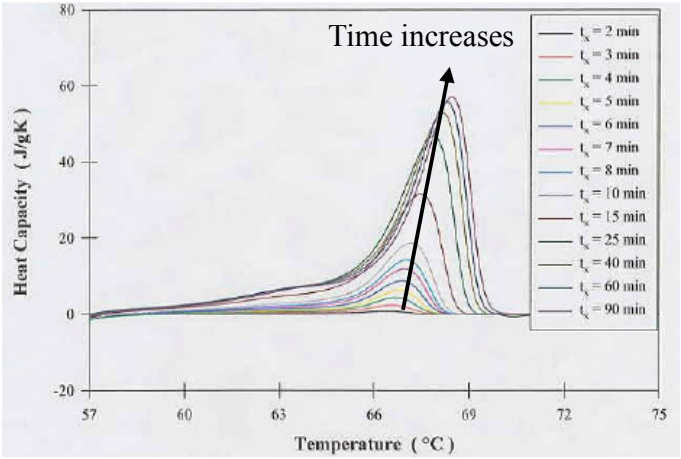

Figure 2.9. DSC melting traces of PEO crystallized at 56.2 °C for different times (adapted from reference 30).

In the case of polymers with relatively low crystallinity, such as semiflexible polymers with large repeat units or polymers with short branches, noncrystallizable comonomers, or stereo- or regio-defects, the melting behavior often exhibits multiple endotherms (Figure 2.10).[7, 30, 31]

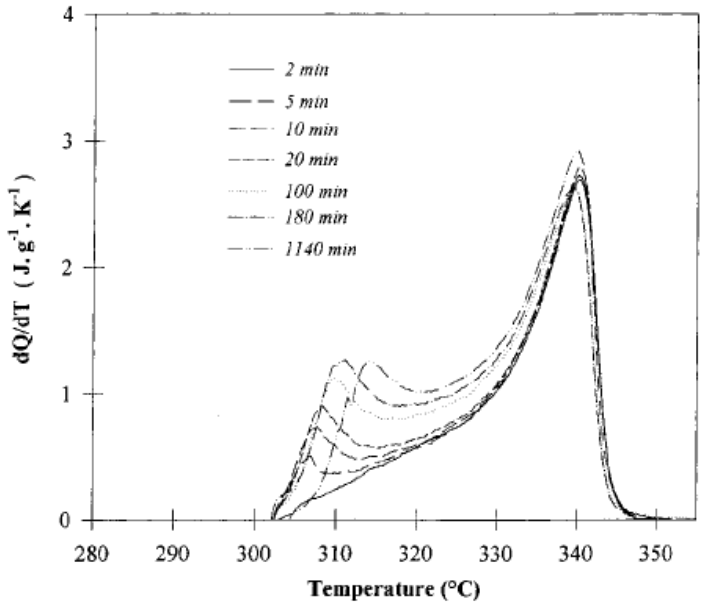

Figure 2.10. DSC melting traces (heating rate of 10 K/min) of PEEK crystallized at 300 °C for different times.[31]

The melting temperature (Figure 2.11) and the heat of fusion (Figure 2.12) associated with the low temperature endotherm increase with crystallization time while these associated with the high temperature endotherm remain constant.

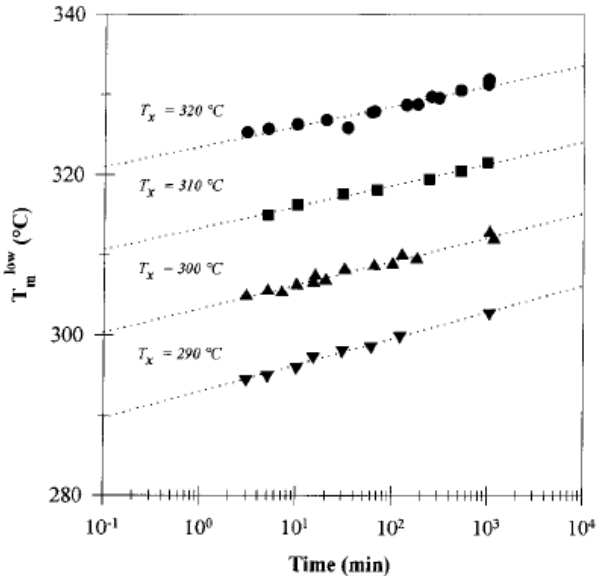

Figure 2.11. Evolution of the low endotherm temperature with crystallization time at different temperatures for PEEK (heating rate of 10 K/min).[31]

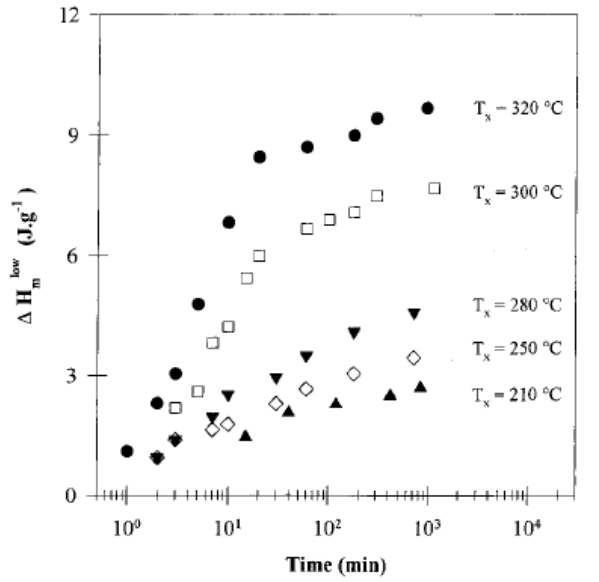

Figure 2.12. Evolution of the low endotherm enthalpy of fusion with crystallization time at different crystallization temperatures for PEEK (heating rate of 10 K/min).[31]

Several models have been proposed for the origin of the double endothermic behavior. Strobl[11, 14] suggested that the low temperature endotherm is associated with the melting of isolated (hence, of lower stability) crystal blocks, while the high temperature endotherm corresponds to the melting of crystal blocks that have merged (more stable). The increase in low endotherm temperature with time arises as a result of crystal perfection. The formation of isolated and merged crystal blocks is described in Figure 2.8.

Another model, proposed a decade ago by Marand and coworkers[7, 30-32] argues that the low temperature endotherm is associated with the melting of secondary crystals, which form predominantly after the growth of primary crystals, and the high temperature endotherm corresponds to the melting of primary crystals (Figure 2.13).

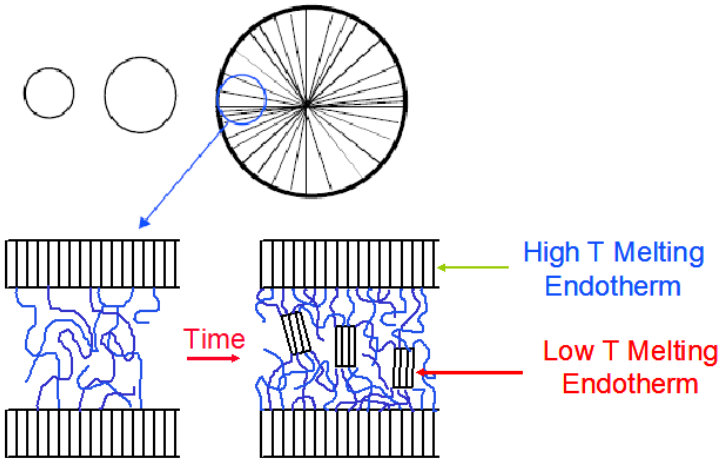

Figure 2.13. Secondary crystal formation model by Marand et al.

(adapted from reference 32).

This model was proposed based on broad and detailed evidence from a large number of

DSC, small angle X-ray scattering, and atomic force microscopy investigations on several semicrystalline polymer systems: EO-copolymers;[7] PEEK;[31, 33-37] bisphenol-A polycarbonate (BAPC) ;[30, 38] poly(ethylene terephthalate) and ethylene-styrene interpolymer;[32] isotactic polypropylene, it-PS, and nylon-6 (unpublished work by Marand's group). Evolution of the heat of fusion with crystallization time led to Avrami exponents in the range of 2 to 4 for the high temperature endotherm, and around 0.5 for the low temperature endotherm. Different crystallization mechanisms were thus proposed to explain the different behaviors of the high temperature endotherm (melting of primary crystals) and the low temperature endotherm (melting of secondary crystals). A melting study of low molecular weight BAPC using heating rate in the range of 5 to 20 K/min showed unambiguously that the multiple melting behavior was associated with a melting-recrystallization-remelting process (see below).[38] However, a similar study with high molecular weight BAPC in a somewhat larger range of heating rates (2.5 to 20 K/min) indicated that the shape and position of the high temperature endotherm were not significantly affected by the change in heating rate, suggesting that melting-recrystallization-remelting process did not occur on the time scale associated with heating in the DSC. The other possibility, that melting-recrystallization-remelting occurred too fast to be observed even at 20 K/min heating, was dismissed at the time, based on the assumption that the rate of melting-recrystallization-remelting should decrease with increasing molecular weight. Furthermore, comparative DSC[31] and real time small angle X-ray scattering (SAXS)[33] studies of PEEK crystallized from the glass or from the melt did not provide support for the melting-recrystallization-remelting mechanism.

To explain the frequently observed multiple melting behavior, a number of investigators have often quoted the melting-recrystallization-remelting mechanism.[39-41] This mechanism proposes that the low temperature endotherm is associated with the melting of crystals present in the as-crystallized sample (Figure 2.1), while the high temperature endotherm is due to the melting of the material, which has recrystallized during the heating scan above the low temperature endotherm. Until recently there has been very little evidence to support this mechanism, because, as stated in the above paragraph, heating experiments using conventional rates in the range of 1 to 40 K/min in a calorimeter or even in a small angle X-ray scattering or wide angle X-ray diffraction set-up had generally failed to show significant heating rate effects. The recent development of nano-calorimeters by Allen et al.[42, 43] and their improvement by Schick et al., [44-47] now allows melting traces to be recorded at heating rates up to 10^6 K/s. A melting study[47] of it-PS showed that the lower and upper endotherms merge into a single endotherm, when the heating rate reaches ca. 100 K/s (Figure 2.14). A similar conclusion was reported for PET for a heating rate of ca. 1000 K/s.[39]

One of the major assumptions made in the elaboration of the secondary crystal formation model was that with a proper choice of the heating rate, it is possible to identify whether or not melting-recrystallization-remelting occurs. Limited by the techniques that were available a decade ago, changing the heating rate by an order of magnitude (such as 5-40 K/min for PEEK and 2.5-20 K/min for BAPC) was thought to be sufficient to identify the reorganization of crystals during heating. Recent chip calorimetry studies suggest that recrystallization occurs extremely rapidly during heating and can only be suppressed with heating rates on the order of

10^2-10^3 K/s or higher.

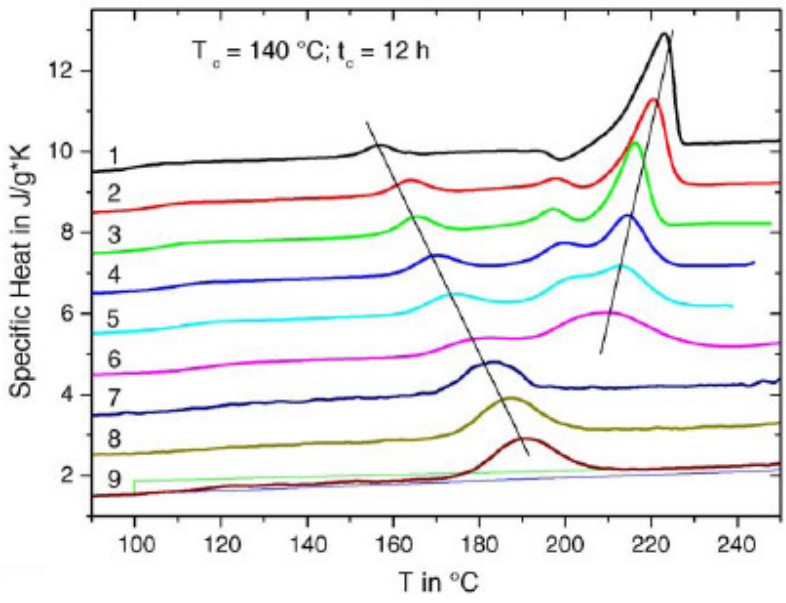

Figure 2.14. Melting of 400 ng to 4 mg it-PS samples at different heating rates: 1) 10 K/min 4 mg; 2) 50 K/min 4 mg; 3) 100 K/min 0.5 mg; 4) 200 K/min 0.5 mg; 5) 400 K/min 0.5 mg; 6) 500 K/min 0.5 mg; 7) 6000 K/min 400 ng; 8) 15,000 K/min 400 ng; 9) 30,000 K/min 400 ng. The samples were crystallized at 140°C for 12 h, cooled to -50°C, and heated at the rate mentioned. The straight lines are guides for the eyes.[47]

2.1.3 Copolymer Crystallization and Melting

This study is specifically focused on statistical copolymers, which are composed of two units: crystallizable A units and non-crystallizable B units. Theoretically, there are two extreme representations for random copolymer crystallization, namely the inclusion and the exclusion

models, which are illustrated in Figure 2.15. In the inclusion model, the copolymer may form a two-phase system with the crystalline phase as a solid solution of A and B units where the co-monomer B units act as defects in the crystalline A lattice. If the defect energy is sufficiently small, both phases have the same composition. In the exclusion model, the copolymer forms a two phase system with the crystalline phase composed entirely of A units and the amorphous phase composed of a mixture of A units and noncrystallizable B units.

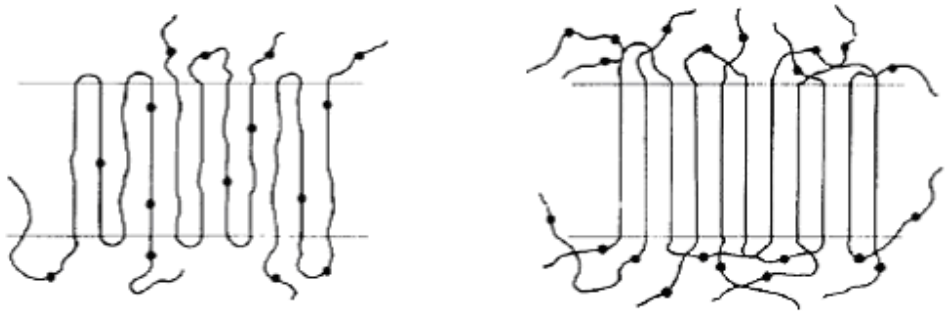

Figure 2.15. Inclusion model (left) and exclusion model (right) (adapted from reference 49).

Flory's thermodynamic equilibrium theory of random copolymer crystallization[48-51] considers the case where B units are defects that are completely excluded from the crystalline A lattice. Based on Flory's theory, the equilibrium melting temperature of a copolymer, T_m, is related to T^0_m, the equilibrium melting temperature of the parent (A) homopolymer:

$$1/T_m - 1/T^0_m = -(R/\Delta H_u) \ln p \qquad (2.5)$$

where, R = gas constant, ΔH_u = the heat of fusion per mole of unit of A, and p = the probability that an A unit is succeeded by another A unit without being influenced by the nature of the

preceding unit.

From Equation 2.5, it is obvious that the equilibrium melting temperature in Flory's theory does not depend on the chemical nature of the B units. The decrease in melting temperature and crystallinity due to copolymerization is only related to the amount of B units and is not influenced by the chemical nature of the noncrystallizable comonomer.

2.1.4 Crystallization, Melting and Morphology of Ethylene/1-Octene Copolymers

Mandelkern's group[52] investigated the crystallization and melting behavior of different kinds of ethylene copolymers. For ethylene/α-olefin copolymers, except for the copolymers containing propylene as a comonomer, the melting temperature is independent of the chemical nature of the comonomer, as long as a sequence distribution is well approximated by the binomial distribution (random copolymerization). Several properties such as the density, the enthalpy of fusion, and the crystallite thickness are found to decrease steadily with increasing comonomer content. These properties are highly dependent on co-unit concentration but independent of co-unit type. Peeters et al.[53] reported that increasing the octene content decreases the crystallization and melting temperatures, crystallinity, spherulite radius, long period, and crystalline lamellar thickness. On the basis of these studies, one can conclude that ethylene/1-octene copolymers follow Flory's exclusion model.

The EO-copolymers studied in the present work were prepared at the Dow Chemical Company using the constrained geometry catalyst (metallocene) technology (CGCT). The

microstructures of EO-copolymers made by CGCT differ significantly from these of copolymers made by conventional Ziegler-Natta catalysts. Conventional Ziegler-Natta catalysts are heterogeneous in nature. Hence, they have multiple active sites with different reactivity ratios for ethylene and various α-olefins. The copolymers produced by Ziegler-Natta catalysts have broader molecular-weight distributions (MWD) and short-chain branching distribution (SCBD). On the other hand, constrained geometry catalysts, and metallocene catalysts in general, exhibit a single active site that controls the composition distribution. In addition, CGCT allows the addition of vinyl-ended polymer chains to produce long-chain branching (LCB). Benefits of LCB are improved processability, shear sensitivity for high-rate extrusion, and melt strength for film stability and drawdown in film-blowing applications. Figure 2.16 illustrates the molecular structure of three ethylene/α-olefin copolymers: conventional linear low density polyethylene (LLDPE) made by Ziegler-Natta catalyst, homogeneous copolymers made by other metallocene technology catalysts (MTC's), and substantially linear homogeneous copolymers made by CGCT.[54]

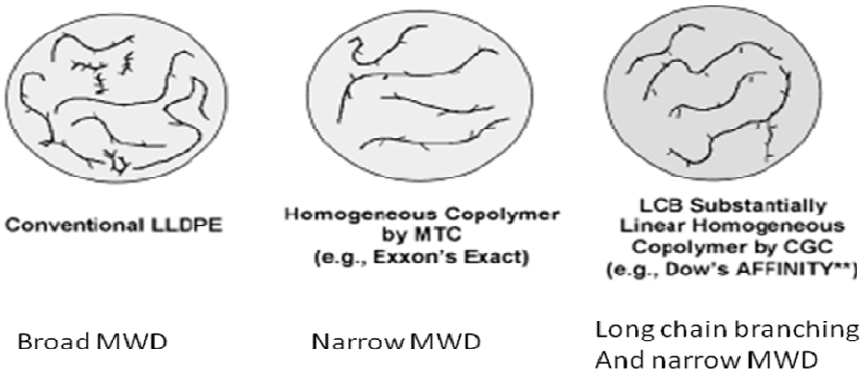

Figure 2.16. Molecular structure comparisons for three different ethylene copolymers (adapted from reference 54).

A study by Moet et al.[55] showed that CGCT ethylene/1-octene copolymers can be classified into one of four groups (Figure 2.17). Type IV materials exhibit a lamellar morphology with well-developed spherulites. Type III copolymers form smaller spherulites with thinner lamellae than the homopolymer. For type II copolymers, spherulites, which contain both bundled crystals and lamellar crystals, are poorly developed and unbanded. Type I copolymers are those with low degree of crystallinity, low melting temperature, absence of cooling rate effects, absence of spherulites and the granular, and nonlamellar morphology.

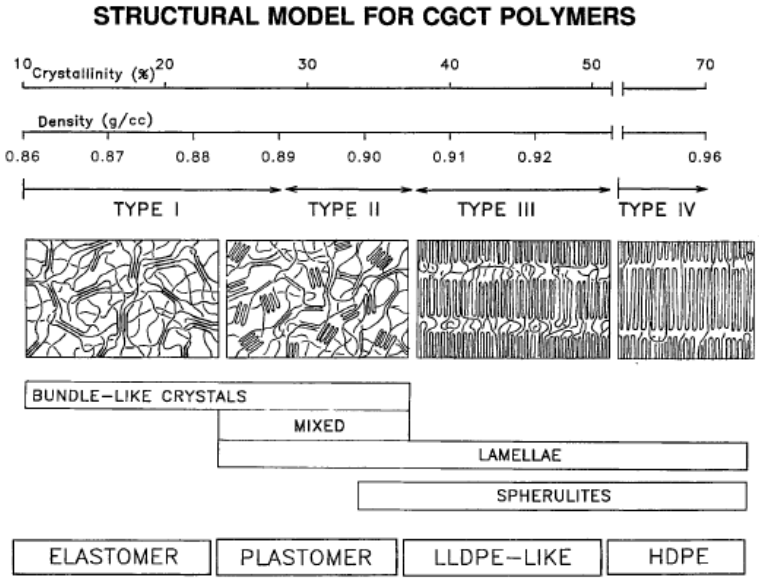

Figure 2.17. Four types of CGCT copolymers (adapted from reference 55).

2.2 Physical Aging

When an amorphous polymer is rapidly cooled to a temperature, T, below the glass transition temperature, T_g, its physical properties are observed to depend on the residence time at T. The change in the physical properties with time are the result of a change in the physical state of the material and indicates that a material below its glass transition temperature is generally in a non-equilibrium state.[56, 57] The change in properties with time is called "physical aging" to distinguish it from the chemical aging generally associated with thermal degradation, photo-oxidation, etc. During physical aging, a material is gradually evolving toward the equilibrium liquid state.[58, 59] Several attempts to describe the origin of physical aging have been offered. Kovacs suggested that the origin of physical aging is related to the evolution of the polymer's free volume, as shown in Figure 2.18.[60] At temperatures below the glass transition temperature (T_g), the specific volume and mobility of the amorphous phase decrease with time. In other words, the non-equilibrium state gradually approaches the equilibrium state.

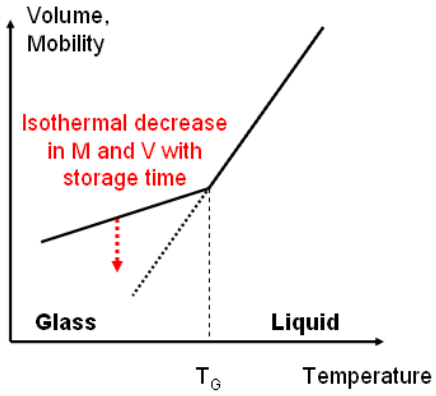

Figure 2.18. Volume-temperature plot around the glass transition temperature (adapted from reference 60).

Creep is a widely used method for studying physical aging. Struik performed a substantial amount of pioneering work on physical aging.[61-66] Struik has shown that at low deformations (in the linear viscoelastic regime) and below T_g, the creep compliance curves (measured here in tension) for different aging times can be superimposed on one reference aging time by shifts along the time axis to make a master curve. When plotting the shift factor a_{ta} versus the aging time, t_a, on a double logarithmic graph, a straight line is obtained. The slope of this line is known as the shift rate or the aging rate, μ, as shown in Figure 2.19.

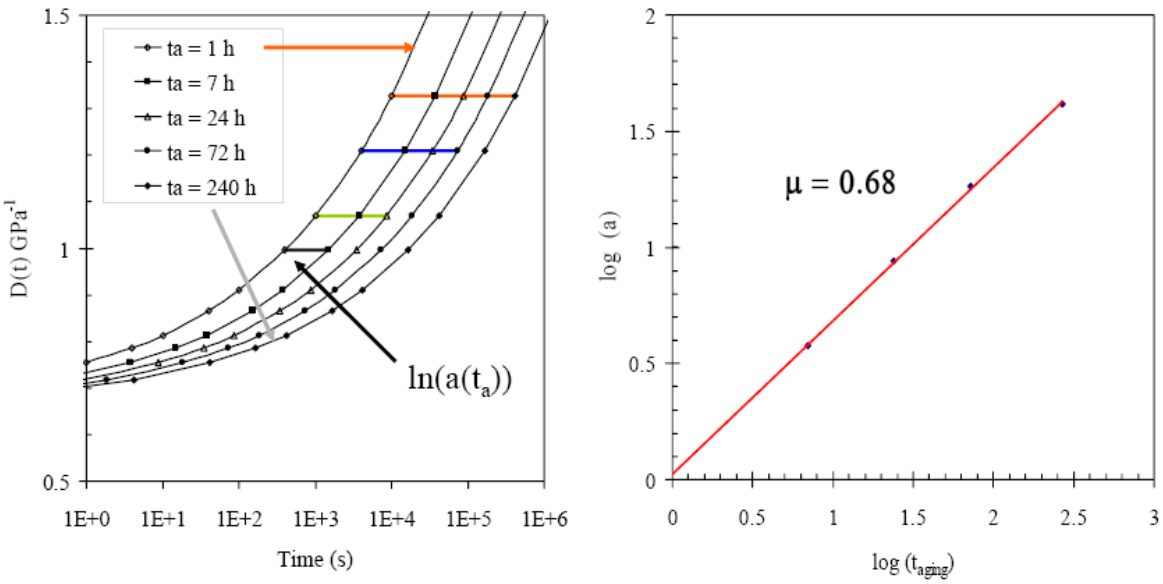

Figure 2.19. Aging rate obtained from tensile creep data.[70]

Semicrystalline polymers have a non-negligible amorphous component and exhibit strong aging effects below their glass transition temperature. Rather unexpectedly, however, they also show strong aging behavior above their glass transition temperature, as shown for isotactic polypropylene (it-PP) at room temperature (Figure 2.20).[63] During aging, changes in compliance

as large as 40-60% can be observed (Figure 2.21).[71]

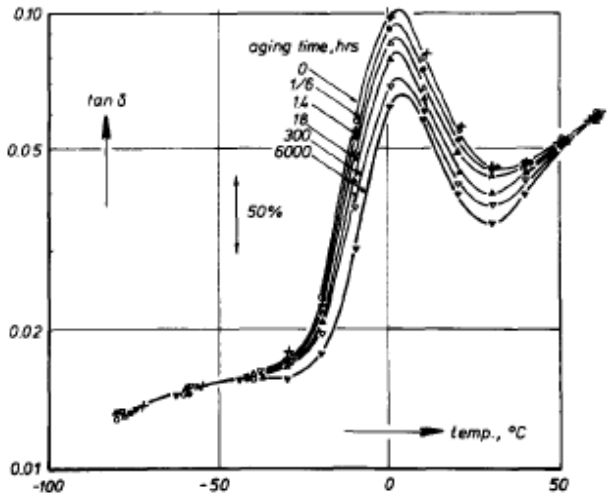

Figure 2.20. Semi-log plot of tan δ (1 Hz) for it-PP after different aging times at 23 °C.[63]

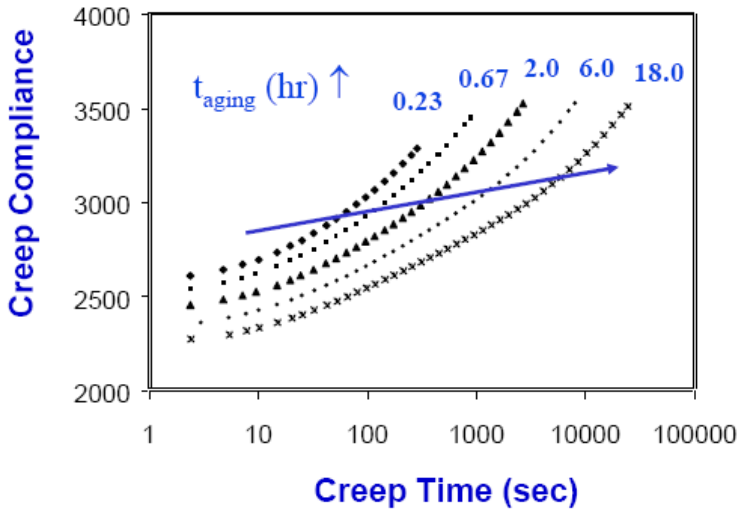

Figure 2.21. Creep behavior of isotactic poly(propylene) aging at 70 °C (adapted from reference 71).

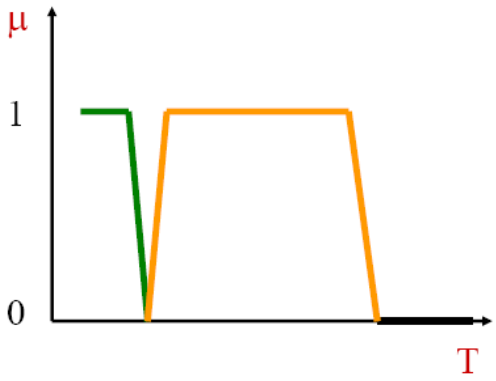

Figure 2.22. Idealized aging rate, μ, vs. temperature for semicrystalline polymers.[70]

It is important to know the relationship between the aging rate and the temperature. An idealized plot of aging rate μ versus temperature is shown in Figure 2.22. To explain the observation of different regimes of aging at different temperatures, Struik proposed the model of an extended glass transition.[62-65] According to Struik, the constraints exerted on the amorphous chains by the crystalline fraction causes a distribution of T_g values, between a lower T_g (T_g^L), identifiable with the nominal T_g of the amorphous polymer, and an upper T_g (T_g^U), which is the T_g of the amorphous fraction most constrained by the proximity of the crystalline lamellae. The aging rates are different in the three regions defined by T_g^L and T_g^U. There is no aging above T_g^U since above T_g^U the entire amorphous fraction is mobile. Between T_g^L and T_g^U both the constrained and relaxed amorphous fractions exhibit aging, while only the mobile amorphous fraction ages below T_g^L. Figure 2.23 illustrates Struik's model.

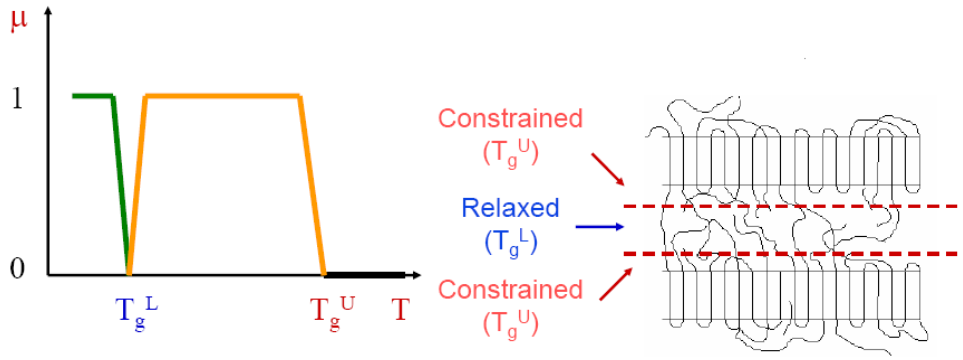

Figure 2.23. Struik's model of physical aging.[70]

Struik's work is pioneering but may be inadequate for semicrystalline polymers. He assumes that during aging there is no change in the shape of the relaxation spectrum (Figure 2.24). McCrum[67] and Read[68] suggest that creep curves for different aging times cannot be superimposed on one reference aging time by only shifts along the time axis because the shape of the relaxation spectrum does change (Figure 2.25). The relaxation strength ($\Delta D = D_R - D_U$) decreases due to the fact that the relaxed compliance (D_R) decreases more than the unrelaxed compliance (D_U) during aging. Since aging affects D_U, D_R and ΔD, it will also affect the calculated shift factor, a_{ta}.

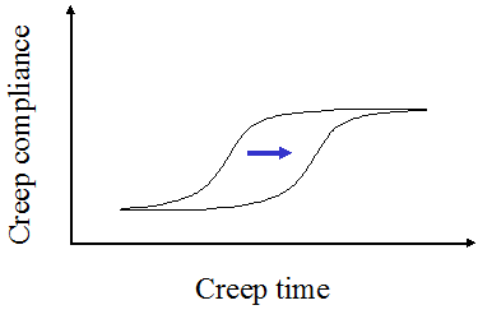

Figure 2.24. Evolution of creep compliance with time (Struik's model) (adapted from reference 67).

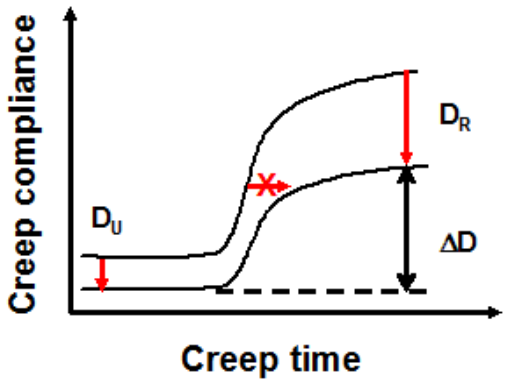

Figure 2.25. Evolution of creep compliance with time (McCrum and Reads' model) (adapted from reference 67).

DSC may be another method to study physical aging. DSC has been used in the past to study the physical aging of amorphous glasses. Hodge et al. discussed the enthalpy relaxation phenomenon in amorphous materials, and the observed shift in the enthalpy recovery peak with aging temperature and time.[72-78] Crystallization studies of semicrystalline polymers also lead to the formation of an endothermic transition some 10 to 30 K above the crystallization temperature. Several studies[7, 30, 31] suggest that for a given crystallization temperature (T_x), the peak temperature of the low temperature endotherm, T_m^{low}, increases linearly with the logarithm of crystallization time (Figure 2.26). We can define parameters $A(T_x)$ and $B(T_x)$ for each crystallization temperature by:

$$T_m^{low}(T_x) = T_x + A(T_x) + B(T_x)\log(t_x) \qquad (6)$$

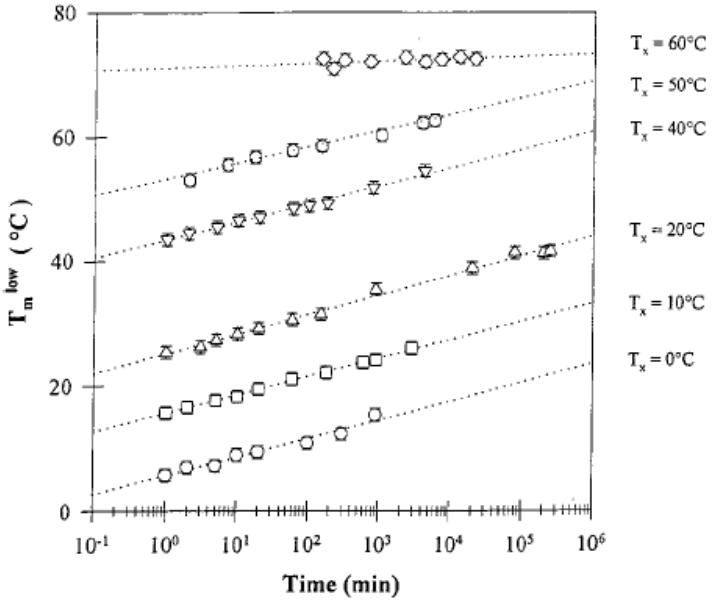

Figure 2.26. Evolution of the low temperature endotherm position with time between 0 °C and 60 °C for ethylene/1-octene copolymer with 12.3 mol% octene.[7]

Theoretically, there are three ways to explain the change in any property P of a semicrystalline polymer with time: 1) a change in the crystalline phase only; 2) a change in the amorphous phase only; 3) a change in both phases. In this work, we suggest that physical aging above the glass transition temperature involves both the crystalline and amorphous fractions. That is

$$P(t) = X_c(t)\, P_c(t) + X_a(t)\, P_a(t) \qquad (2.7)$$

In contrast to Struik, who considered that aging above T_g is only associated with a densification of the constrained amorphous phase, Marand et al.[7, 30-32] suggested that physical aging is a consequence of secondary crystal formation, a process, which affects both the crystalline and amorphous phases. In this model, secondary crystals would act as cross-linking

sites for the remaining amorphous segments, hence, cause the observed evolution of the mechanical properties. The change in the mechanical properties is due to both the change in $X_c(t)$ and the change in $P_a(t)$ (due to the increase in constraints for isotropic materials). Secondary crystallization is associated with the formation of new crystals only below a cross over temperature, T_{CO}, defined in Figure 2.27.[30]

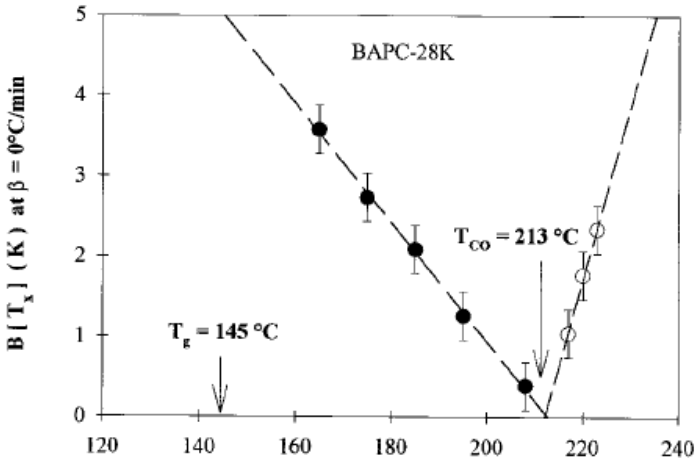

Figure 2.27. Definition of the cross-over temperature (T_{CO}) from the crystallization temperature T_x dependence of $B(T_x)$ for BAPC.[30]

In Figure 2.27, they plot $B(T_x)$, the slope of $T_m^{low}(t)$ vs. log t, determined for different crystallization temperatures. When the crystallization temperature increases toward T_{CO}, $B(T_x)$ is observed to decrease. Above T_{CO}, no secondary crystals form, and the melting behavior is characterized by a single melting endotherm. The mechanism of secondary crystallization above T_{CO} was speculated to be the thickening of existing lamellae. A possible correlation was offered between T_{CO} and the α_c relaxation temperature, $T_{\alpha c}$, above which the rapid cooperative segmental motion in the crystal phase allows the lamellar thickening process to occur at a measurable rate.

This led Marand et al.[7, 30] to suggest that physical aging may originate from the lack of mobility in both the crystal and the amorphous phases. The entropic constraints caused by secondary crystals can only be released if segmental motion takes place sufficiently rapidly and over large enough length scales in both the amorphous and the crystal phases (Figure 2.28).

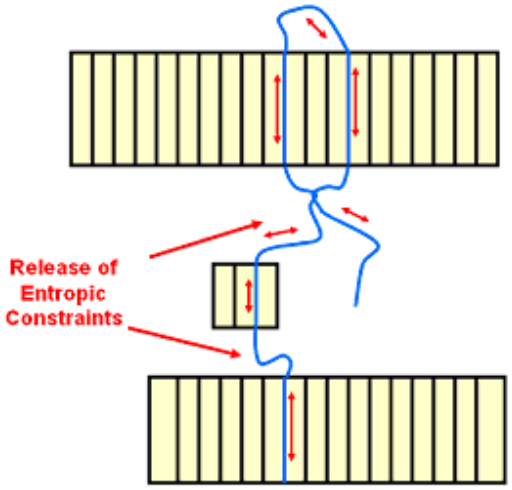

Figure 2.28. Marand's model of physical aging: segmental mobility below T_{CO}.[70]

Since the onset of segmental mobility for the crystal and amorphous phases is associated with the temperatures, T_{CO} and T_g, respectively, it was proposed that the segmental mobility at the crystal/liquid interphase is controlled by a reduced temperature, denoted Θ, defined by Equation 2.8.

$$\Theta = \frac{T_{CO} - T_x}{T_{CO} - T_g} \tag{2.8}$$

The lower T_x, the larger Θ, and the lower the mobility. Thus, the influence of secondary crystallization on the remaining amorphous fraction is larger at lower temperature. Consequently, at lower temperatures, the rate at which the conformational constraints can be released is slower.

Thus, the rate at which the physical properties of the remaining amorphous fraction are expected to change with time is larger. One of the unpublished results from Marand's group (Figure 2.29) shows that the variation of B with θ seems to follow the same trend for BAPC with different molar masses, PET, it-PS, and PEEK. This data suggests some universality in the behavior of semicrystalline polymers with regard to aging between T_{CO} and T_g.

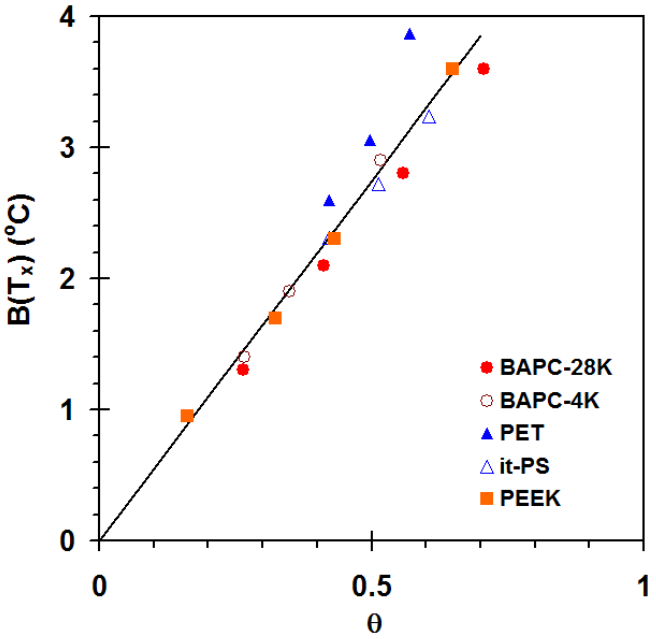

Figure 2.29. Evolution of B as a function of the dimensionless temperature, θ.[79]

However, the mechanism proposed by Marand et al.[7, 30] suggest that physical aging should stop as soon as the production of secondary crystals ceases. This requirement is not supported by the data on Figure 2.30, which shows that the low endotherm heat of fusion increases quickly at short crystallization times, but increases very slowly at very long crystallization times ($t > 10^3$ minutes). This observation is not consistent with the assumption that the number of constraints

(caused by the secondary crystals) increases steadily with the logarithm of time, even at long crystallization time.

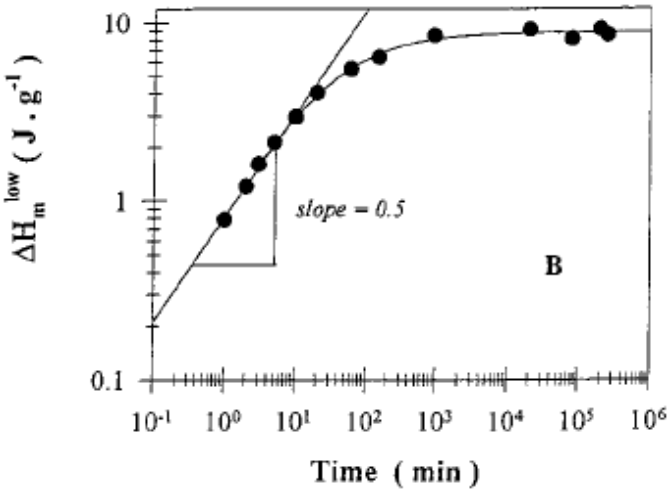

Figure 2.30. Evolution of the low endotherm heat of fusion for EO-12.3 after crystallization at 20^{o}C for different times.[7]

Chapter 3. Experimental

3.1 Materials

The ethylene/1-octene (EO)-copolymers investigated in this study were synthesized at the Dow Chemical Company using the CGCT INSITE^{TM} technology.[54] The materials, along with their octene content, weight average molecular weight (M_w), polydispersity index (PDI), and density, are listed in Table 3.1.1. All values in the table were provided by the Dow Chemical Company. The comonomer composition in EO-copolymers were determined by temperature rising elution fractionation (TREF).[80-82]

Table 3.1.1 Characteristics of EO-copolymers.

Sample Name	Octene Content, (mol%)	Octene Content, (wt%)	M_w (g/mol)	PDI	Density (g/cm^3)
EO-3.4	3.37	8.30	116000	2.34	0.9103
EO-8.2	8.22	17.63	100800	2.15	0.8873
EO-12.3	12.3	22.99	119700	2.04	0.8726

3.2 Methodology

The main goal of this thesis is to investigate the effect of long isothermal treatment above T_g on the physical properties of semicrystalline EO-copolymers. The principal experimental technique for these investigations is the differential scanning calorimetry (DSC). Additional studies focused on properties such as the density and the small strain creep compliance.

3.2.1 Differential Scanning Calorimetry

3.2.1.1 Conventional Differential Scanning Calorimetry

A TA Instruments Q2000 DSC was used under dry nitrogen purge. Since metals have a much higher thermal conductivity than organic materials, using a pure indium sample as a standard to calibrate the temperature scale is not suitable. Indium and tin "sandwiches", made by inserting a piece of indium or tin between two pieces of polymer films, were used to serve as calibration standards. Thin films were prepared by melt pressing at 160 °C in a Carver laboratory hot press in a dry nitrogen atmosphere and were subsequently quenched in cold water. Small samples with similar masses (1.2 ± 0.2 mg) were used to minimize and simplify thermal lag corrections.

3.2.1.2 Rapid Heating Cooling Differential Scanning Calorimetry

The DSC thermograms at fast heating rates were recorded using a RHC DSC from TA Instruments under dry nitrogen purge. The heating rates are 50, 250, 500, 1000 and 1500 K/min. Samples size are in the range of 100~200 μg.

3.2.2 Density

Densities of EO-copolymers were measured at 23.00 ± 0.05 °C in a Techne DC-1 density gradient column prepared using isopropanol and water. Since the density range of

EO-copolymers is 0.87-0.92 g/cm^3, 1080 mL isopropanol/water solution (with a density of 0.82 g/cm^3) and 920 mL pure water were used to prepare the density gradient column. Calibration of the column was carried out with 8 standard floats whose densities are known within ± 0.0001 g/cm^3. The resolution of the column was about 0.0002 g/cm^3. Measurements were carried out at least twice with fresh samples cut from compression-molded films to ensure reproducibility.

3.2.3 Creep Behavior

Creep measurements are widely used to study physical aging.[61-66] The small strain creep study was carried out in bending mode on a TA Instruments model 2980 Dynamic Mechanical Analyzer. The aging behavior was studied at 30 °C, which is well above the glass transition temperature of each EO-copolymer (-55 °C, -46 °C and -33 °C for EO-12.3, EO-8.2 and EO-3.4, respectively) and below the T_{CO} (94 °C, 103 °C, and 110 °C, for EO-12.3, EO-8.2 and EO-3.4, respectively, as will be shown in Section 4.1.1.3). The creep studies were performed using a methodology well described in the literature.[56, 61-66] The aging times were 0.11 hour, 0.33 hour, 1 hour, 3 hours, and 9 hours. After an initial aging time t^1_{aging}, a small constant stress was applied during the creep time t_{creep}. The resulting bending creep compliance J(t) was recorded. The ratio of t_{creep} to aging time t_{aging} was smaller than 0.17 to minimize the effect of aging during the creep measurement period and get a "snapshot" of the properties at t_{aging}. Then the load was released and the sample was allowed to recover. The recovery time was about 15 times t_{creep} to obtain a complete recovery of the strain. At the time $t^{(i+1)}_{aging} = 3t^{(i)}_{aging}$, the constant stress was

applied again to start the next creep cycle. Figure 3.1 illustrates the process. To make sure the creep test was done in the linear viscoelastic response region, the applied stress was sufficiently small that the strain was typically less than 0.1%.

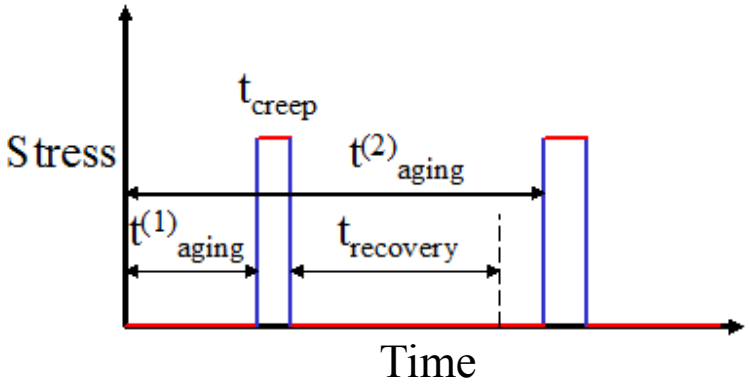

Figure 3.1. Creep test schedule for aging studies (adapted from reference 56).

Chapter 4. Results and Discussion

4.1 Results

4.1.1 Differential Scanning Calorimetry

Section 4.1.1.1 examines the effect of crystallization time and temperature on the development of the low temperature endotherm. Section 4.1.1.2 examines the effect of octene content on the development of the low temperature endotherm. Section 4.1.1.3 investigates the relationship between rate of shift of the low endotherm and the reduced temperature, while Section 4.1.1.4 discusses the evolution of DSC crystallinity as a function of time.

4.1.1.1 Effects of Crystallization Time and Temperature

We record the melting behavior of ethylene/1-octene copolymers crystallized isothermally at varying temperatures for different crystallization times. A sample is initially rapidly heated to 160 °C, where it is kept for 2 minutes to erase any previous thermal history. The sample is then cooled at 20 K/min to a temperature, T_x, where it is allowed to crystallize isothermally for a certain amount of time. Next, the sample is subsequently quenched to a temperature 40 K below the crystallization temperature. The sample is subsequently melted at a rate of 10 K/min.

Figure 4.1 shows a typical set of DSC heating scans for EO-12.3 crystallized at 23 °C for different times. At about 62 °C, each heating scan shows a high temperature endotherm (T'_m). These endotherms exhibit almost the same position and shape. In the temperature region below

T'_m, a low temperature endotherm is observed above the temperature of isothermal treatment, T_x. The magnitude and position of the low temperature endothermic peak increase with crystallization time, t_x. The shift of the low temperature endothermic peak to higher temperatures is proposed to be associated with the melting-recrystallization-remelting and crystal perfection.

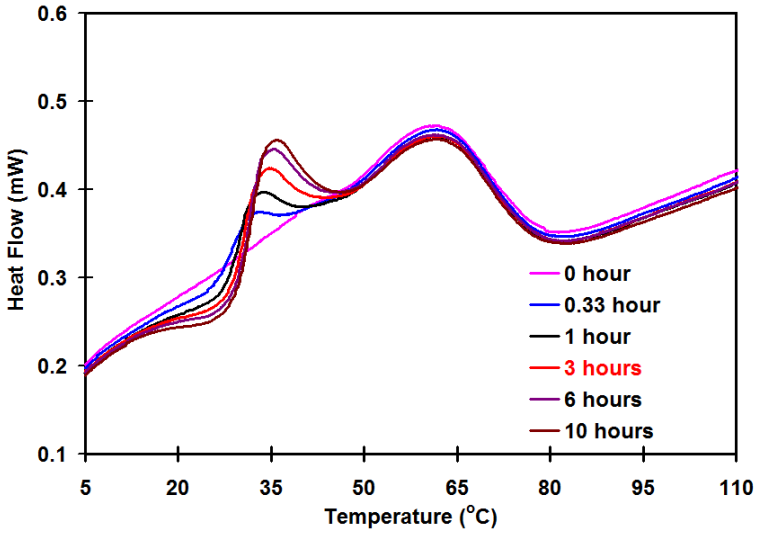

Figure 4.1. Evolution of the melting behavior of EO-12.3 after quenching from 160 to 23 °C, residence at 23 °C for various times and subsequent quenching to -17 °C.

To determine the peak position of the low temperature endothermic transition, the heat flow curve obtained for the 0 hour residence time at 23 °C is used as "baseline". The heating traces are obtained after subtraction of the baseline and display a negative deviation from zero with a minimum around T_x, 23 °C (Figure 4.2.A). Then, a positive deviation with a maximum is displayed at about 8 K above the minimum. The maximum of the low temperature endothermic transition for the subtracted heat flow curve is defined as $T_m^{low}(t_x)$. Figure 4.2.B shows that a

more negative deviation is observed in the subtracted DSC traces below 23 °C when crystallization time increases. As the crystallization time increases, fewer amorphous sequences are available for crystallization during the subsequent quench from 23 °C to -17 °C.

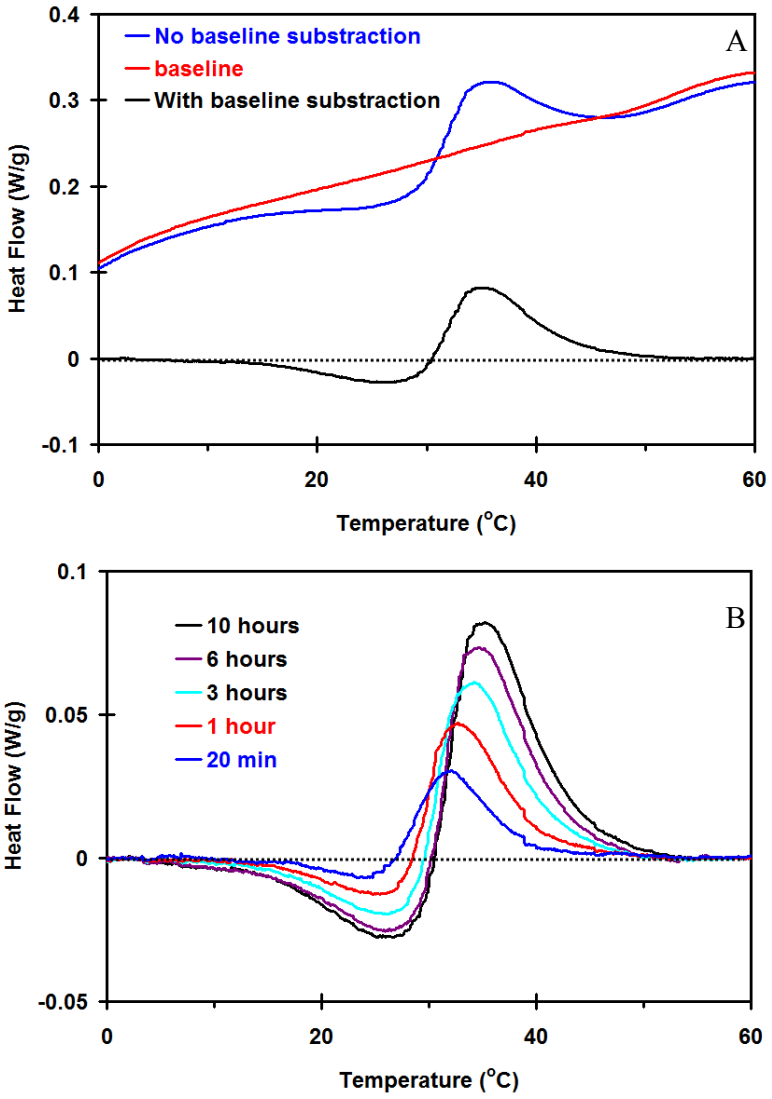

Figure 4.2. Evolution of the low temperature endotherm of EO-12.3 after quenching from 160 to 23 °C, residence at 23 °C for various times and subsequent quenching to -17 °C. (A) Example of baseline subtraction for 10 hours crystallization; (B) DSC traces after subtraction for various crystallization times.

We now focus on the effect of the crystallization temperature. Figure 4.3 shows DSC heating scans (at a heating rate of 10 K/min) of EO-12.3, which was allowed to crystallize at different temperatures (random order) for 10 hours. Similar to Figure 4.2, at about 62 °C, each heating scan shows a high temperature endothermic peak ($T_m^{'}$). The upper endotherm exhibits almost the same position and shape. A low temperature endothermic peak is observed above T_x. Magnitude of the low temperature endothermic peak increases with an increase of T_x. T_m^{low} is on a line, which is almost parallel to the $T_m^{'} = T_x$ line on the Hoffman-Weeks plot (Figure 4.4).[5]

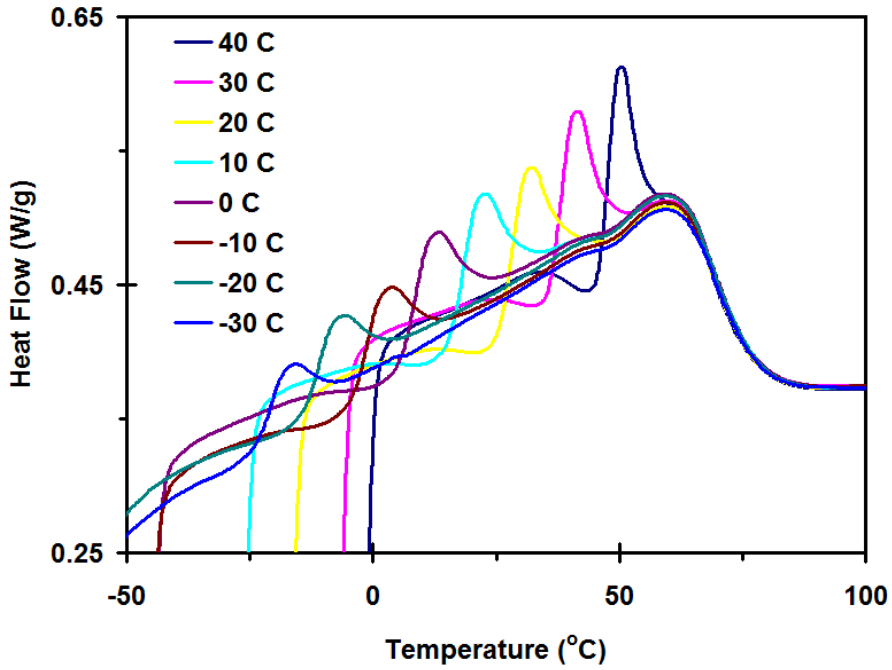

Figure 4.3. DSC heating scans of EO-12.3, crystallized for 10 hours at various temperatures.

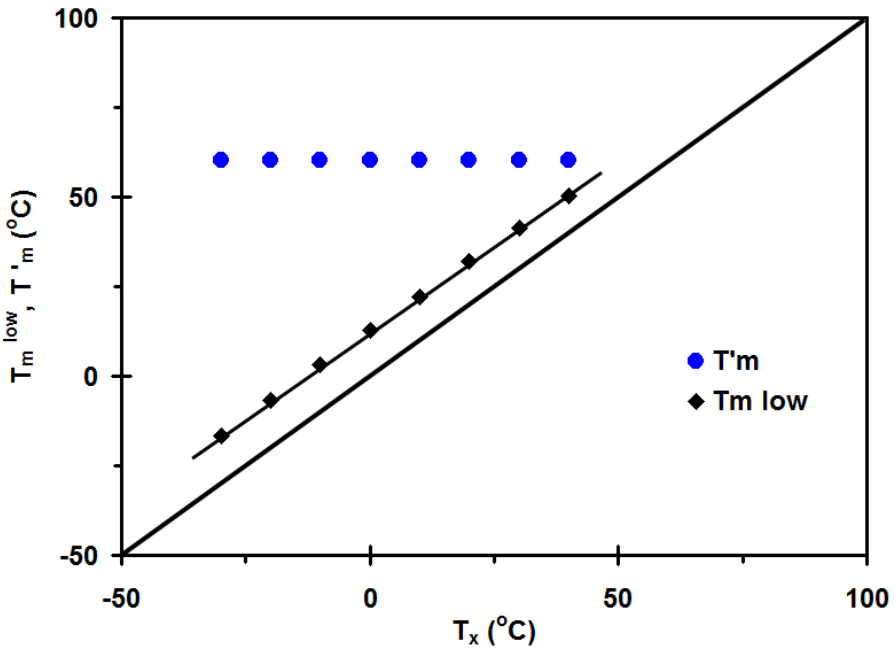

Figure 4.4. Evolution of T_m^{low} with crystallization temperature T_x (crystallized for 10 hours).

Earlier studies of the isothermal crystallization of the EO-copolymers (Figure 11 in Reference 7) suggested that the logarithmic time scale must be chosen to effectively investigate the time dependence of the low temperature endotherm. T_m^{low} is plotted in Figure 4.5 for various crystallization temperatures and times for EO-12.3. In all cases, T_m^{low} increases linearly with $\log(t_x)$, as represented by Equation 4.1:

$$T_m^{low} = T_x + A(T_x) + B(T_x) * \log(t_x) \qquad (4.1)$$

where the parameters A and B are functions of T_x.

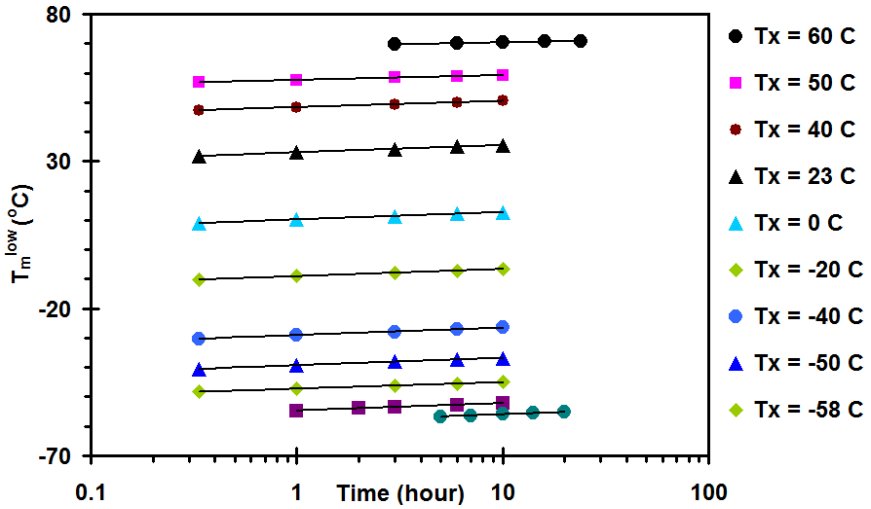

Figure 4.5. Variation of T_m^{low} for various temperatures as a function of time for EO-12.3.

$B(T_x)$ is the slope of the linear plot of $T_m^{low}(t)$ vs. log(t) at a given crystallization temperature, T_x. The evolution of $B(T_x)$ with T_x is investigated over a wide temperature range for EO-12.3 (Figure 4.6). As Figure 4.1 shows, a significant decrease of $B(T_x)$ is observed for $T_x \geqq 40$ °C. On the other hand, when the sample is crystallized at successively lower temperatures, $B(T_x)$ decreases to reach a minimum at $T_x \sim T_g$. Further lowering the temperature below -60 °C leads $B(T_x)$ to a constant value. The evolution of $B(T_x)$ with T_x is shown in Figures 4.7 and 4.8 for EO-8.2 and EO-3.4, respectively. The low temperature crystallization study by DSC was carried out only for EO-12.3, since the low temperature endothermic peak is too small to yield a reliable value of T_m^{low}, hence, of $B(T_x)$ for EO-3.4 and EO-8.2.

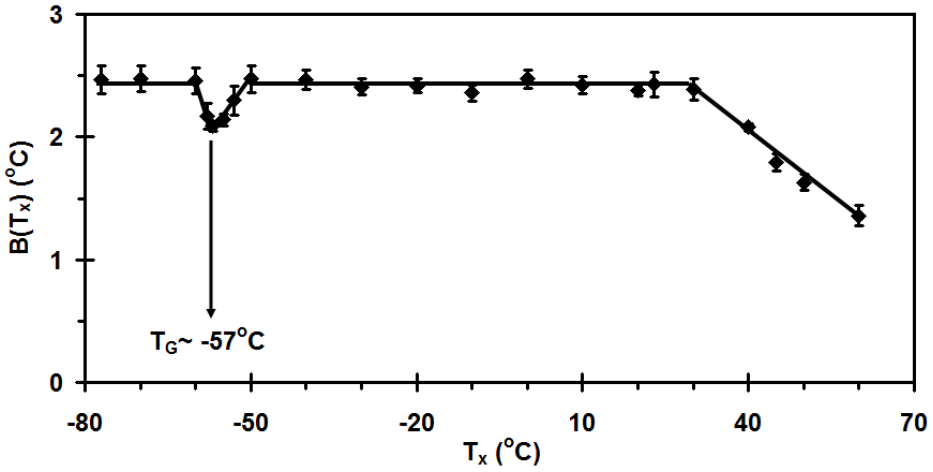

Figure 4.6. Evolution of $B(T_x)$ with T_x for EO-12.3 (cooling at 20 K/min and heating at 10 K/min).

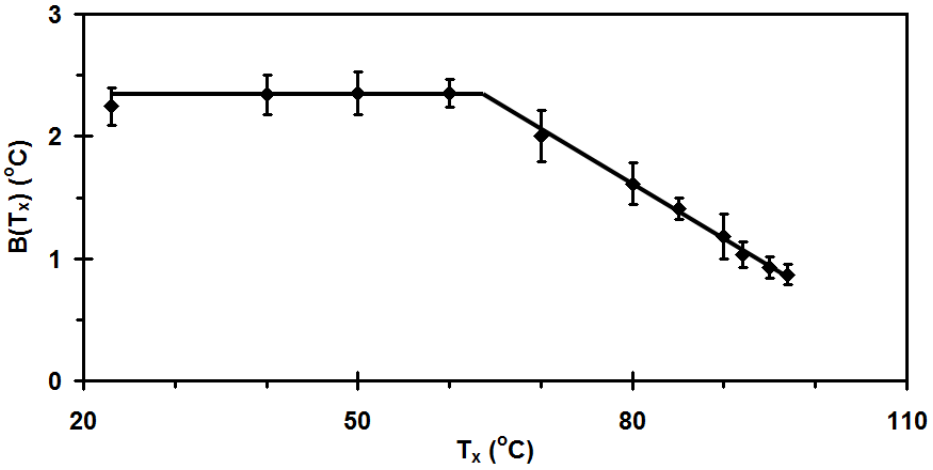

Figure 4.7. Evolution of $B(T_x)$ with T_x for EO-8.2 (cooling at 20 K/min and heating at 10 K/min).

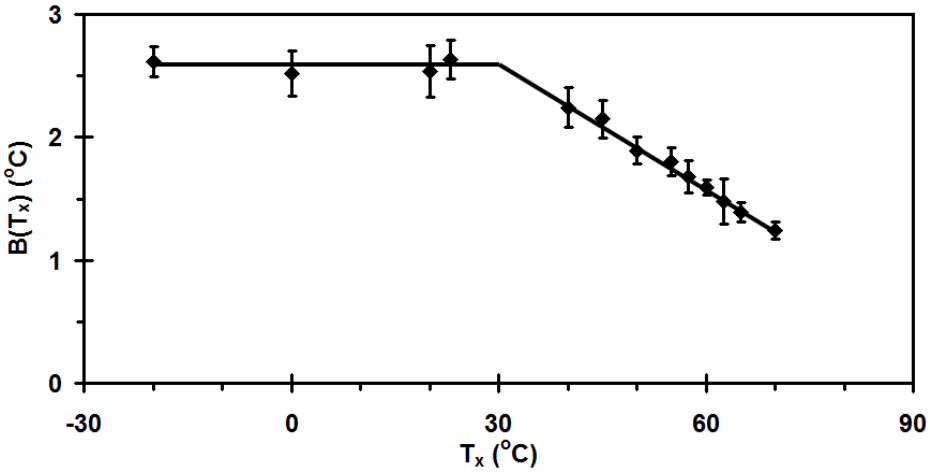

Figure 4.8. Evolution of $B(T_x)$ with T_x for EO-3.4 (cooling at 20 K/min and heating at 10 K/min).

4.1.1.2 Effects of Octene Content on the Development of Low Temperature Endotherm

Changing the octene content changes the physical properties of the EO-copolymers. Decreasing the octene content increases T_g, increase the crystallinity, and increases melting temperatures of the high temperature endothermic peak. This study only focuses on the effect of octene content on the development of the low temperature endothermic peak. As observed in a previous study in our laboratory (Figure 1 in reference 7), the relative magnitude of the lower temperature exotherm increases with octene content over the range of copolymer compositions considered here. The DSC crystallization study was carried out at the same temperature as the density experiment, specifically at 23^{o}C, (see Section 4.1.2 for details). As shown in Figure 4.9, $B(T_x)$ of EO-8.2 is the largest among the three EO-copolymers. These results will be compared with the results obtained from density measurements in the following discussion section.

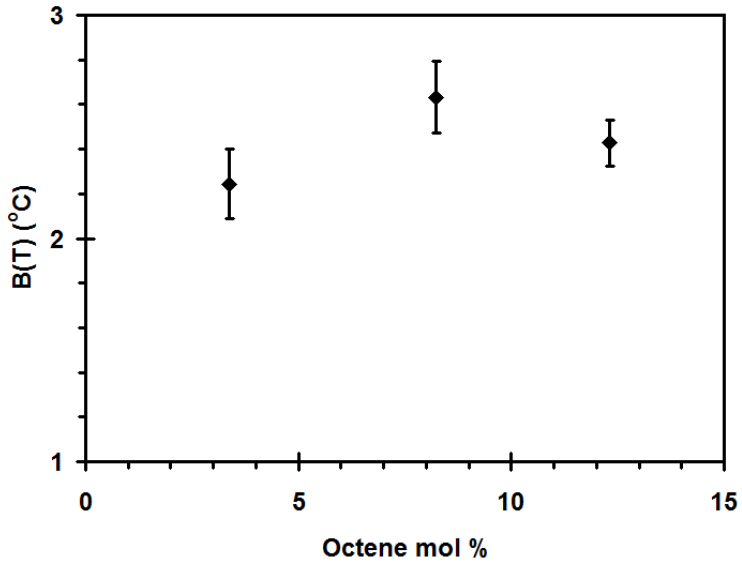

Figure 4.9. B(T_x) vs. octene mol% at 23°C.

4.1.1.3 B as a Function of the Reduced Temperature θ

As discussed at the end of Section 2.2, the reduced temperature, θ, is calculated using Equation 2.8. B(T_x) is measured at different heating rates and then is extrapolated to zero rate to yield B(T_x, HR=0). Then, extrapolation of the B(T_x, HR=0) vs. T_x plot to the condition B(T_x) = 0 allows to define the cross-over temperature, T_{CO}. The T_g and T_{CO} values for EO-copolymers are given in Table 4.1.1. T_{CO} decreases when the octene content increases. This is explained by a reduced local concentration of crystallizable -CH_2-CH_2- sequences. One of the unpublished results from Marand's group (Figure 2.29) shows that the change of B(T_x) with reduced temperature, θ, appears to exhibit universal behavior, where BAPC of different molar masses, PET, it-PS, and PEEK data at different temperatures fall on the same curve. Similarly the reduced temperatures of three EO-copolymers are calculated using Equation 2.8 and are shown

in Figure 4.10. The black line in Figure 4.10 is the best fit of data from PEEK, it-PS, BAPC, and PET (Figure 2.29). It is independent of the nature of the polymer as long as the reduced temperature is used.

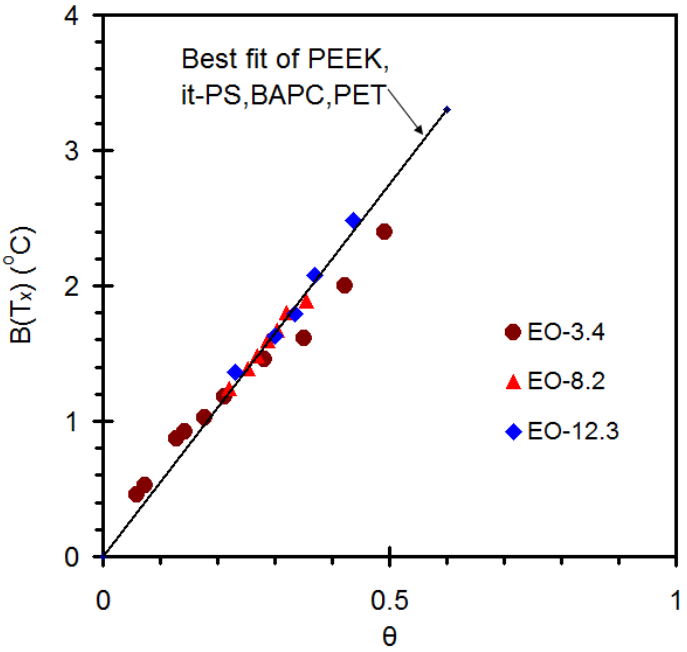

Figure 4.10. Change of segmental mobility with $B(T_x)$ for three EO-copolymers.

Table 4.1.1 T_g and T_{CO} of EO-copolymers

Sample	Octene Content (mol%)	T_g (°C)	$^*T_{CO}$ (°C)
EO-3.4	3.37	-33	111
EO-8.2	8.22	-46	103
EO-12.3	12.3	-52	94

* Obtained by extrapolation of $B(T_x)$ to zero heating rate and zero DSC aging rate.

4.1.1.4 Crystallinity

A fractional degree of crystallinity based upon DSC data, X_c^{DSC}, is calculated from the following equation:

$$X_c^{DSC} = \frac{\Delta H_m}{\Delta H_m^0} \tag{4.2}$$

where the experimental data ΔH_m is the observed melting enthalpy of a sample, and ΔH_m^0 is the heat of fusion for completely crystalline linear polyethylene (290 J/g).[83] For EO-12.3, ΔH_m is calculated by an integration of the DSC heating trace over the temperature interval from 5°C to 85°C. The crystallinity is 0.0965 at zero crystallization time and increases slowly with an increase of crystallization time (Figure 4.11).

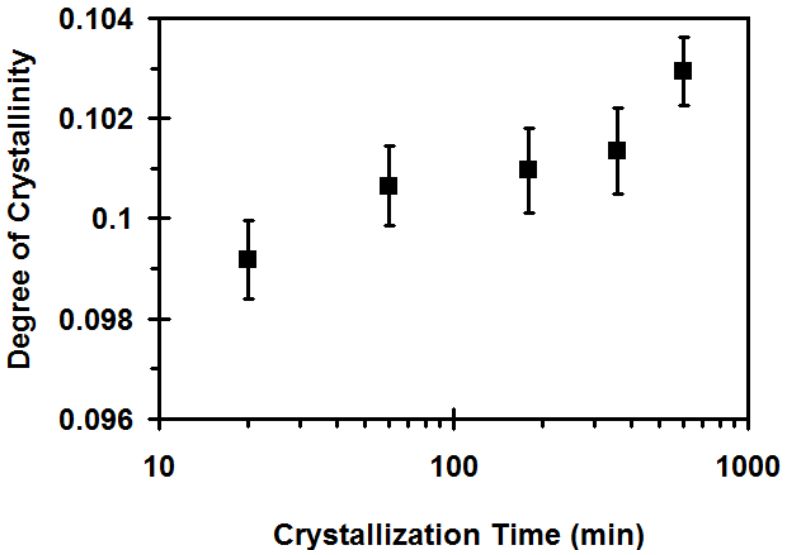

Figure 4.11. Evolution of the DSC fractional degree of crystallinity with residence time at 23°C for EO-12.3.

4.1.2 Density

4.1.2.1 Effect of Octene Content

The evolution of the sample density with the crystallization time at 23°C is investigated and plotted in Figures 4.12, 4.13, and 4.14 for EO-3.4, EO-8.2, and EO-12.3, respectively. Slopes of density with the crystallization time, D(T), are summarized in Table 4.1.2 and plotted in Figure 4.15.

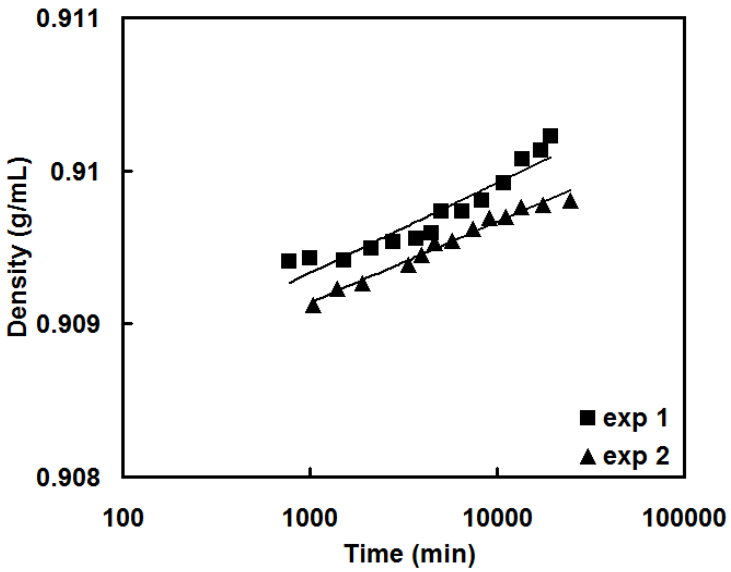

Figure 4.12. Evolution of the density as a function of time at 23 °C for EO-3.4.

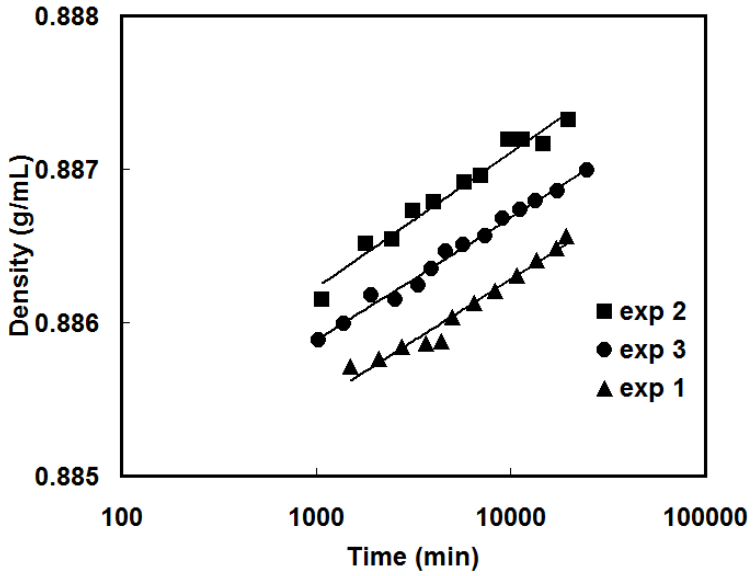

Figure 4.13. Evolution of the density as a function of time at 23 °C for EO-8.2.

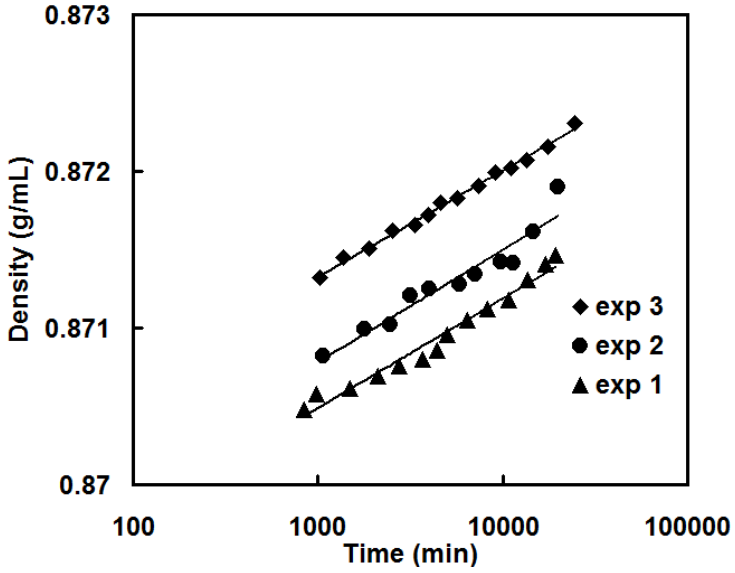

Figure 4.14. Evolution of the density as a function of time at 23 °C for EO-12.3.

Table 4.1.2 Summary of the slopes of density vs. log t for EO-copolymers at 23°C

Samples	D(T) g/mL
EO-3.4	2.4 ± 0.1
EO-8.2	3.6 ± 0.2
EO-12.3	3.0 ± 0.1

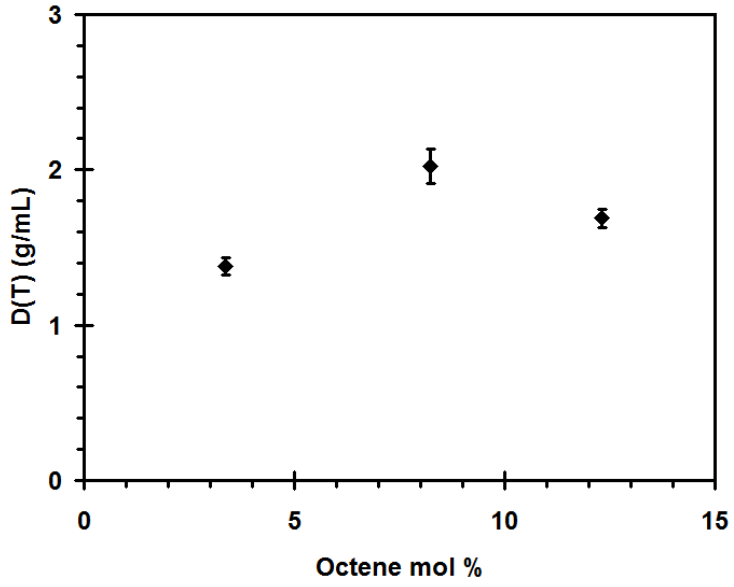

Figure 4.15. Slopes D(T) of density vs log t vs. octene mol% at 23°C.

4.1.2.2 Crystallinity

A fractional degree of crystallinity based upon density, X_c^{Dens}, can be obtained from Equation 4.3:

$$X_c^{Dens} = \left(\frac{\rho_c}{\rho}\right)\left(\frac{\rho - \rho_a}{\rho_c - \rho_a}\right) \quad (4.3)$$

where ρ is the experimental density, $\rho_{c,}$ and ρ_a are the crystalline and amorphous densities, respectively. At 23°C, the values of 1.00 g/cm^3 for the crystalline density and 0.852 g/cm^3 for the amorphous density are often quoted and have been adopted by most investigators.[84-86] Thus, these values are used in this study. X_c^{Dens} of EO-12.3 is calculated and shown in Figure 4.16. While small differences in the absolute value of X_c^{Dens} are observed in multiple density measurements of different samples, all measurements show similar time dependences.

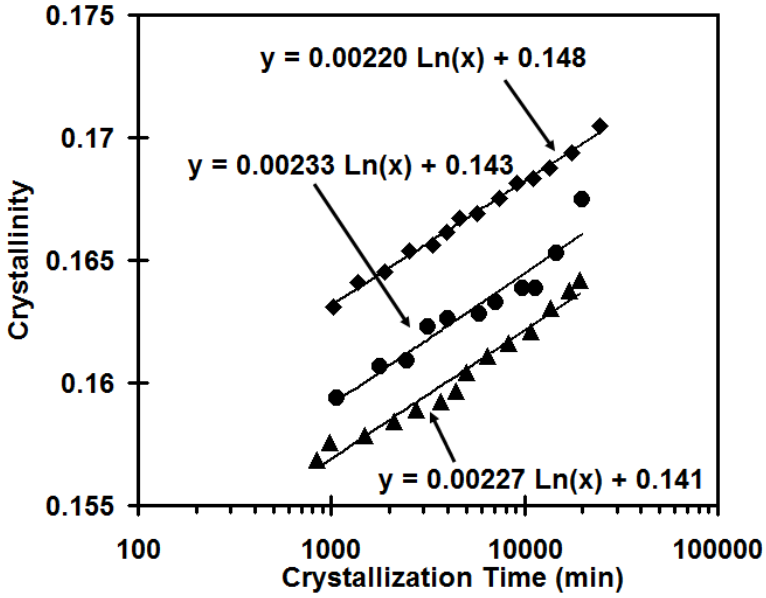

Figure 4.16. Evolution of the fractional degree of crystallinity with residence time at 23°C for EO-12.3 from density measurements.

4.1.3 Creep

4.1.3.1 Effect of Aging Time

Creep measurements are used to study mechanical rates of aging. The creep compliances for the different aging times at 30°C are plotted as a function of creep time in Figures 4.17-4.19 for EO-3.4, EO-8.2, and EO-12.3, respectively. At short aging times (6.7 min and 20 min), the creep compliances increase and then decrease in the creep measurements of all three EO-copolymers. In contrast, at long aging times (1 hour, 3 hours and 9 hours) the creep compliances always increase during the creep measurements. Figures 4.17-4.19 show that the shape of the creep compliance curves changes significantly with aging time. The creep compliance curves obtained at different aging times cannot be superposed by horizontal and/or vertical shifts to obtain a master curve.

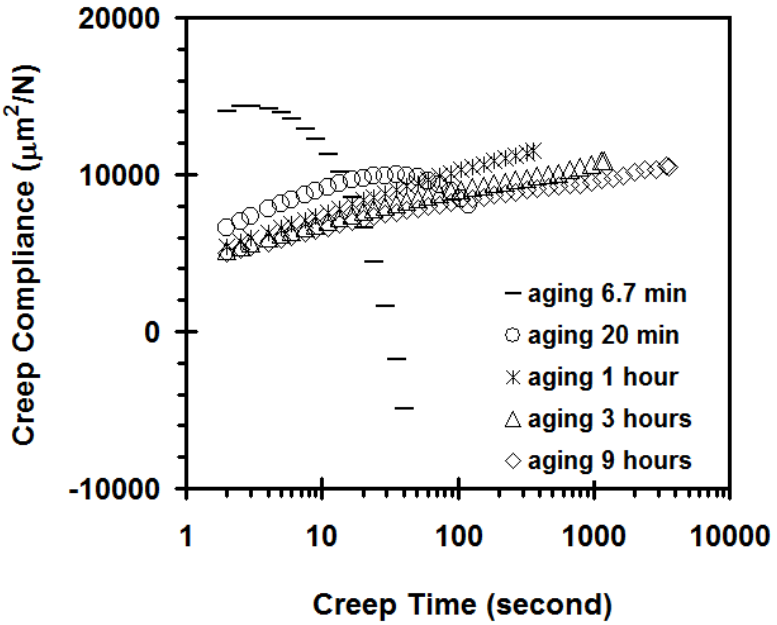

Figure 4.17. Creep study at 30°C for EO-3.4.

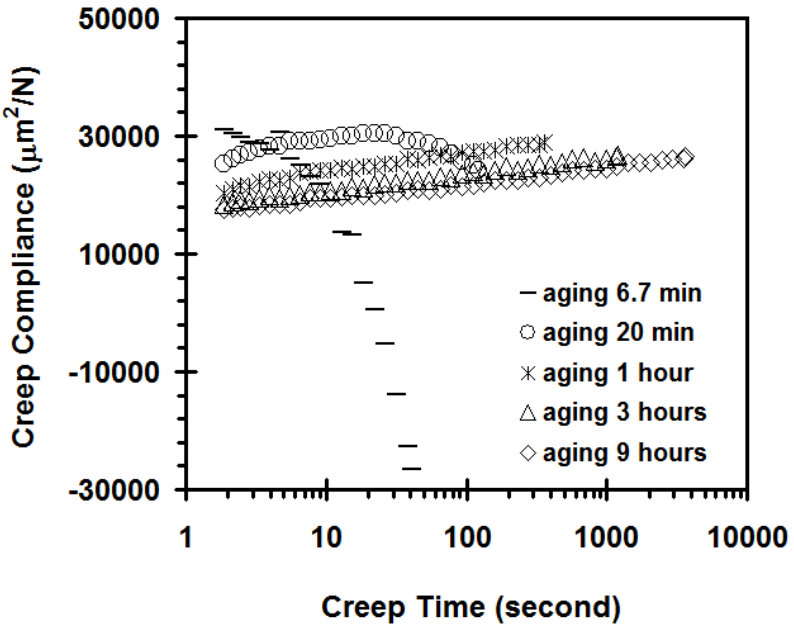

Figure 4.18. Creep study at 30°C for EO-8.2.

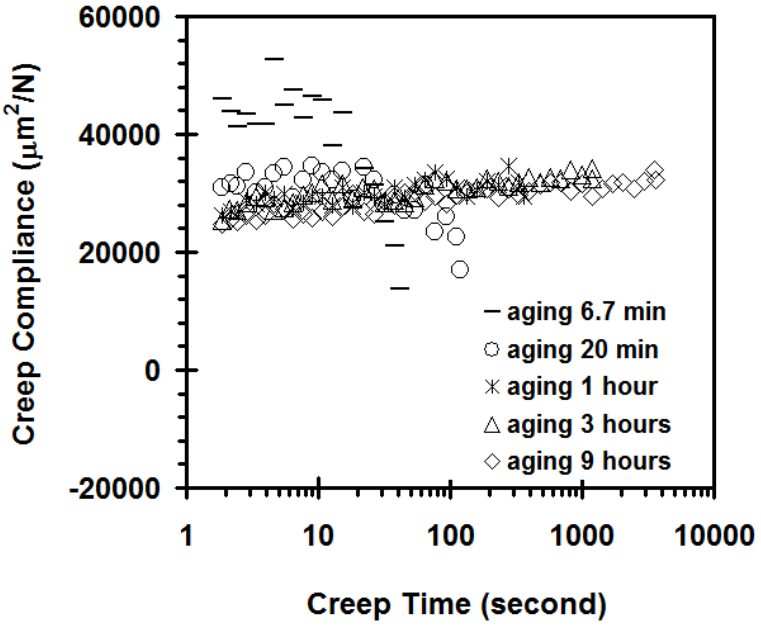

Figure 4.19. Creep study at 30°C for EO-12.3.

4.1.3.2 Effect of Octene Content

Creep compliance vs. creep time curves are plotted in a logarithmic time scale for the three EO-copolymers after a long aging times on Figure 4.20 (1 hour), Figure 4.21 (3 hours) and Figure 4.22 (9 hours). The creep rate, m, is defined as creep compliance divided by logarithmic creep time and is considered to be associated with molecular mobility.[62, 63] Creep rates after long aging times (1 hour, 3 hours, and 9 hours) are plotted as a function of copolymer composition in Figure 4.23.

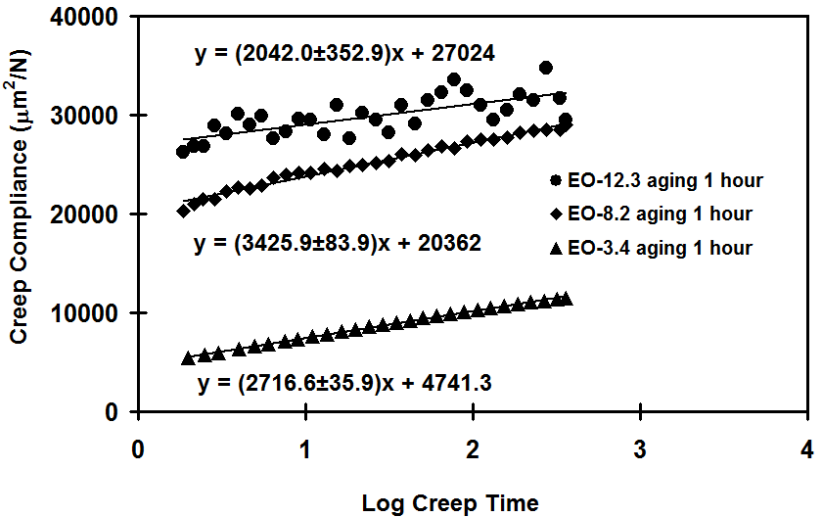

Figure 4.20. Creep study after 1 hour aging.

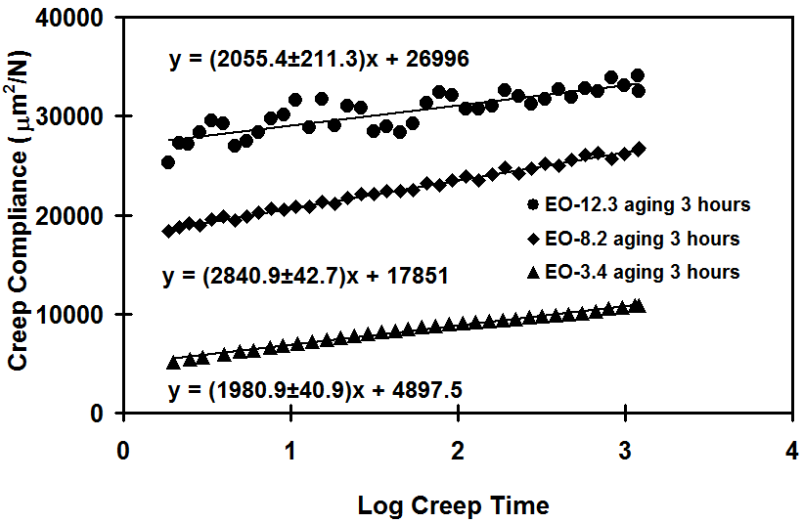

Figure 4.21. Creep study after 3 hours aging.

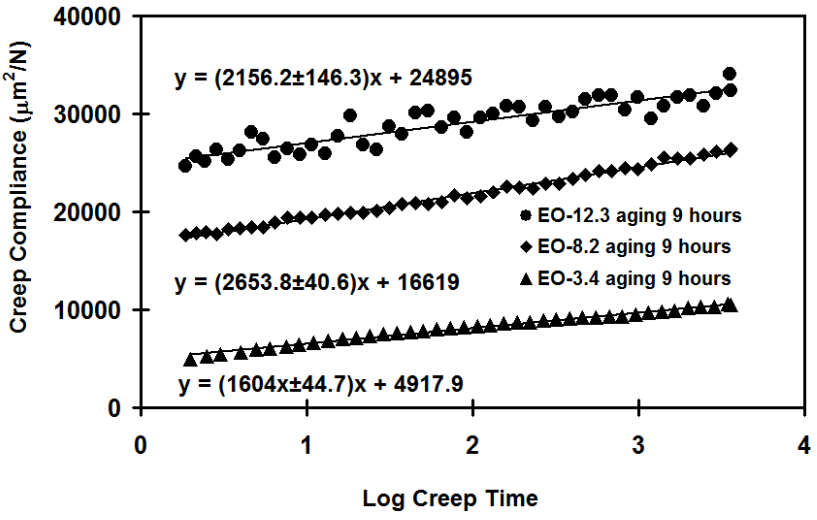

Figure 4.22. Creep study after 9 hours aging.

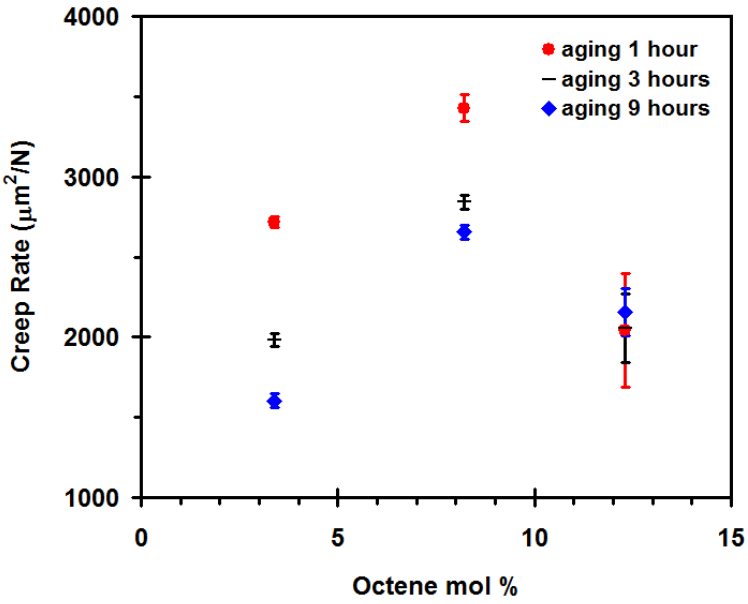

Figure 4.23. Creep rate as a function of copolymer composition for different aging times (1 hour, 3 hours and 9 hours).

4.1.4 Rapid Heating Cooling Differential Scanning Calorimetry

To distinguish between the melting-recrystallization-remelting and the secondary crystallization mechanisms, melting studies of EO-12.3 are carried out at fast heating rates (100, 500, 1000, 1500 and 2000 K/min) after isothermal crystallization (Figure 4.24).

For these experiments, EO-12.3 was first melted at 433.15 K to erase any previously established thermal history. It was than cooled to 233.15 K and held isothermally for 20 minutes followed by quenching to 123.15 K. Finally, the sample was heated to 433.15 K at various heating rates.

For comparisons with results obtained from previous studies, the multiple melting behavior

of PEEK was also studied using the TA Instrument RHC DSC at the following heating rates: 50, 200, 400, 800 and 1200 K/min (Figure 4.25). PEEK samples were first melted at 653.15 K to erase any previously established thermal history. Samples were then cooled to 573.15 K and held isothermally for 15 minutes. Next, the samples were further cooled to 513.15 K and held isothermally for 15 minutes followed by quenching to 173.15 K. Finally, the samples were heated to 653.15 K with different heating rates.

Examination of Figures 4.24 and 4.25 makes it clear that the two melting peaks of EO-12.3 and PEEK start to merge together when the heating rate increases.

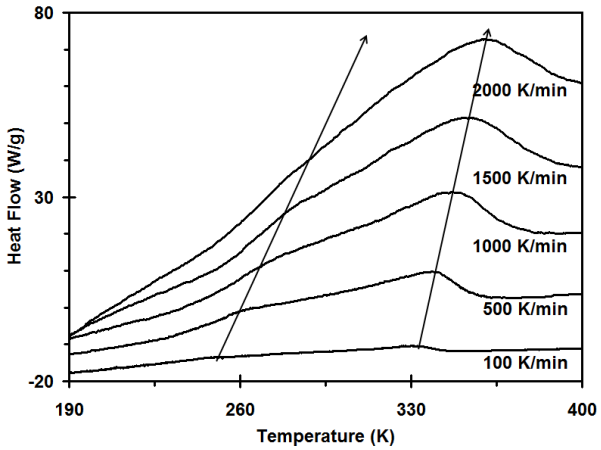

Figure 4.24. Multiple melting behavior of EO-12.3 (crystallizes at 233.15 K for 20 minutes).

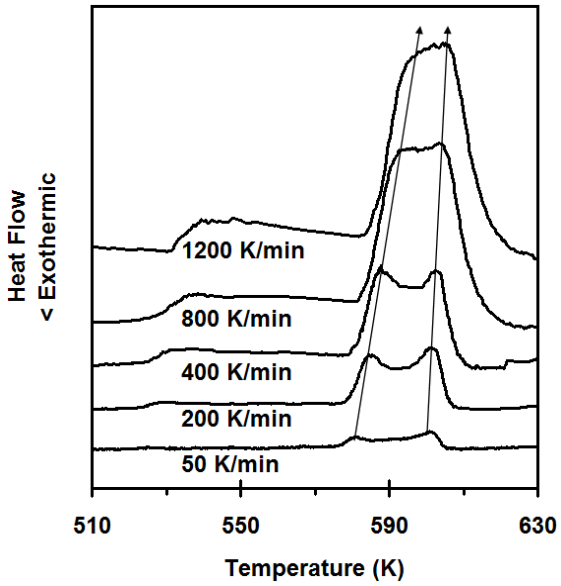

Figure 4.25. Multiple melting behavior of PEEK (crystallizes at 573.15 K for 15 minutes, then quenches to 513.15 K and crystallizes for 15 min).

4.2 Discussion

4.2.1 Development of the Low Temperature Melting Endotherm after Crystallization

A low temperature endothermic peak is observed in the melting scan of semicrystalline EO-copolymers subsequent to crystallization. Both the magnitude and the position of this peak increase with the crystallization temperature and time. The multiple melting behavior is associated with the melting of small and unstable crystals, the recrystallization of the melt produced by their melting, and the melting of the recrystallized material. This conclusion is drawn from the reorganization effects observed in Figures 4.24 and 4.25 and consistent with Schick's findings for PET and it-PS. The low temperature endotherm corresponds to the melting

of these small crystals. The high endotherm is associated with the melting of crystals, which form during the heating scan. With a longer crystallization time, T_m^{low} shifts to a higher temperature, a reflection of the ability of these crystals to stabilize with time. Following the work of Alfonso et al.[87] and Strobl et al.[11, 13, 14], it is likely that the stabilization under isothermal conditions is associated with an increase in lateral crystal dimensions or an increase in crystal perfection rather than with an increase in crystal thickness, since no changes are observed in the angular dependence of the SAXS of these materials during aging.

4.2.2 Evolution of $B(T_x)$ with T_x

$B(T_x)$ is used to define the calorimetric rate of aging by DSC measurements. The change of B with T_x for PEEK, an unpublished result from Marand's group, is shown in Figure 4.26. Note that Figures 4.6 and 4.26 are qualitatively similar to Figure 2.17 for the mechanical rate of aging from Struik's model. $B(T_x)$ is associated with the rate of increase in crystal stability. Small and unstable crystals are formed at a low crystallization temperature. These crystals can rapidly stabilize with time. As T_x increases (and approaches T_{CO}), it is known that crystals are larger and more stable. Thus, their driving force toward stabilization decreases and the rate of increase in stability, $B(T_x)$, decreases. At some temperature, $T_x = T_{CO}$, the crystals formed are sufficiently large, hence, stable, that they melt at a high enough temperature and can no longer undergo melting-recrystallization-remelting. In other words these crystals simply melt. It is indeed expected that the rate of recrystallization should decrease with increasing temperature as high

enough temperatures. Thus, T_{CO}, is the temperature where the melting-recrystallization-remelting processes vanishes. At these high temperatures, segmental mobility increases dramatically in the crystal, and the crystals can still improve their stability with increasing crystallization time at a rate that increases with temperature ($T_x \cong T_{CO}$). Hence, we speculate that the increase in $B(T_x)$ with T_x for $T_x > T_{CO}$ (Figures 2.27 and 4.26) is associated with the thermally activated increase in segmental motion, while the decrease in $B(T_x)$ with T_x for $T_x < T_{CO}$ is associated with a decrease in driving force toward stabilization under conditions where the rate of segmental motion is too low to play a significant role (Figures 4.6-4.8, and Figure 4.26).

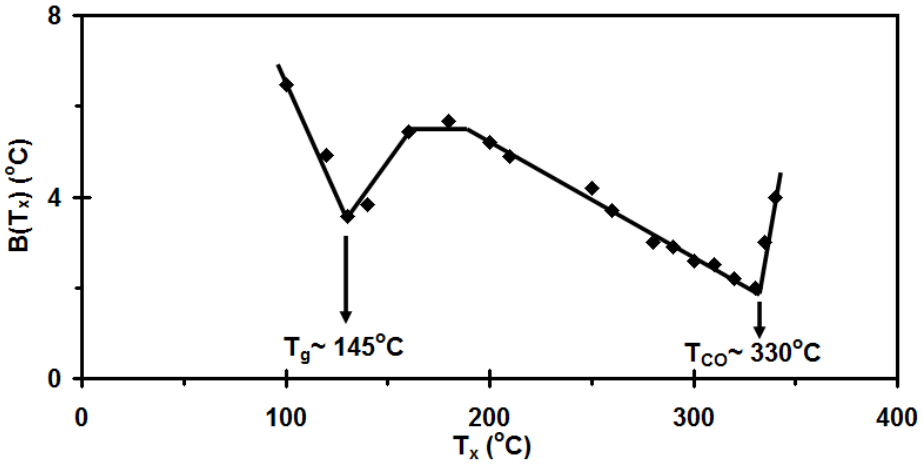

Figure 4.26. Change of $B(T_x)$ with T for PEEK (heating at 10 K/min).[79]

4.2.3 Universality of the B vs. θ Trends for EO-copolymers and Other Semicrystalline Polymers

We note in Figure 4.10 that the rate of stabilization B(T) measured for the three

EO-copolymers studied here follow the same trend as PEEK, it-PS, BAPC, and PET. This observation suggests that similar processes occur at the cross-over temperature, T_{CO}.

4.2.4 Same Trend for the Slopes of DSC and Density Measurements

We also note that at 23°C the DSC (Figure 4.9) and density (Figure 4.15) aging rates exhibit the same copolymer composition dependence (Figure 4.27). Both of these rates can be associated with a stabilization process if an increase in density and melting temperature can be related to an increase in stability. While such correlation is obvious for the melting temperature, it is less so for density, unless the observed increase in density is associated with an increase in lateral crystal dimensions or an increase in crystal perfection. We also note that the rate of stabilization for EO-8.2 is the highest among the three EO-copolymers. The observation that the rate of stability increase is a maximum at intermediate copolymer composition makes sense from the standpoint that copolymers with a very high level of short-chain branching (high octene content), crystallize only to a very limited extent (if at all), hence, their crystals have very limited ability to increase their stability. On the other hand, crystallization of linear chains, or of copolymers with very few short-chain branches, leads to crystals that are almost perfect and have very little driving force toward stabilization. Also, in such materials, crystallization by a chain-folding mechanism leads to very high crystallinity. Hence, in this case, there are very few amorphous segments available for further crystallization. In this case, the rate of stabilization at low temperature approaches zero. Obviously, at higher temperature, a different mechanism may be at play to increase stability

(lamellar thickening). The above consideration can explain why an EO copolymer of intermediate composition (EO-8.2) exhibits the highest rate of stabilization.

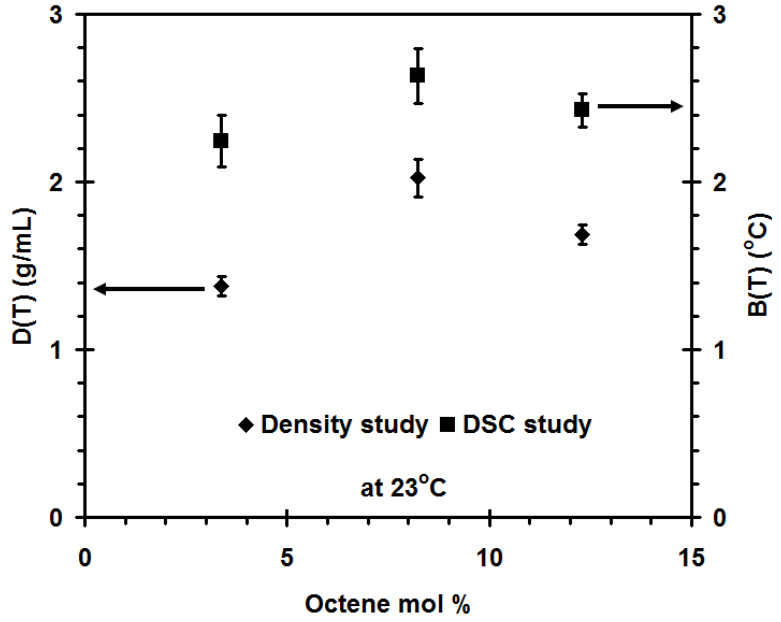

Figure 4.27. Evolution of D(T) and B(T) with octene content by density and DSC measurements.

4.2.5 Increase of Crystallinity with Crystallization Time for DSC and Density Experiments

The crystallinities of EO-12.3 are calculated by equations 10 and 11 for the DSC and the density measurements, respectively. These two methods are the most widely used routine methods of crystallinity determination. Multiple density measurements show different X_c^{Dens} for the same material since the samples are stored at room temperature for different times before carrying out the density measurements. For DSC measurements, the samples are always melted to erase the thermal history before crystallization. It must be noted that for all X_c^{Dens} calculations,

it was assumed that the density of the amorphous phase in the semicrystalline polymer is constant and identical to that of purely amorphous polyethylene – 0.852 g/cm^3. It is not surprising to note that the values of X_c^{Dens} and X_c^{DSC} are somewhat different since samples for density and DSC were kept at room temperature for different times. The key point is that both measurements suggest that the crystallinity increases steadily with crystallization time. This is consistent with a solid-state NMR study of isotactic polypropylene by VanderHart et al.,[88] which suggests that the degree crystallinity of it-PP increases slightly but steadily during aging above T_g, and does not remain strictly constant as hypothesized by Struik.[62-65]

4.2.6 Summary of the Small Strain Creep Results

In order to obtain a "snapshot" of the properties at an aging time t_{aging}, the time scales for the creep tests are set to follow Struik's suggestion for short-time tests (Figure 2.25). Since the ratio of t_{creep} to t_{aging} is smaller than 0.14, the effect of aging during the creep measurement period can be neglected as indicated by Struik.[62,63] However, our creep measurements of EO-copolymers show very different behavior (Figures 4.17-4.19) at various aging times. With an increase in aging time, the constraints associated with the crystallinity increase (crystals act as crosslink points). Thus, the molecular mobility decreases. This explains why the creep rates of EO-3.4 and EO-8.2 decrease with increasing aging time as shown in Figure 4.23 (long aging times). The uncertainty is too large to draw any conclusion from Figure 4.23 for the softer material EO-12.3.

As Figure 2.30 indicates, the crystallinity increases fast in the early stage of crystallization and slows down at later times.[7] Thus, after a shorter aging time (6.7 min or 20 min), the increase of crystallinity can occur rapidly by a variety of mechanisms (new crystal formation in the remaining amorphous phase, an increase in the size of small crystals, and an increase in crystal perfection)[87] and the sample shrinks during the creep test, which explains why a smaller and even a negative creep compliance is obtained at the end of the creep measurement (Figures 4.17-4.19). The change in the creep compliance of EO-8.2 with time is the largest among the three EO-copolymers (Figure 4.28).

This observation is consistent with the DSC and density results which allowed us to conclude that EO-8.2 has the highest rate of stabilization (the largest magnitude for B(T) and D(T)).

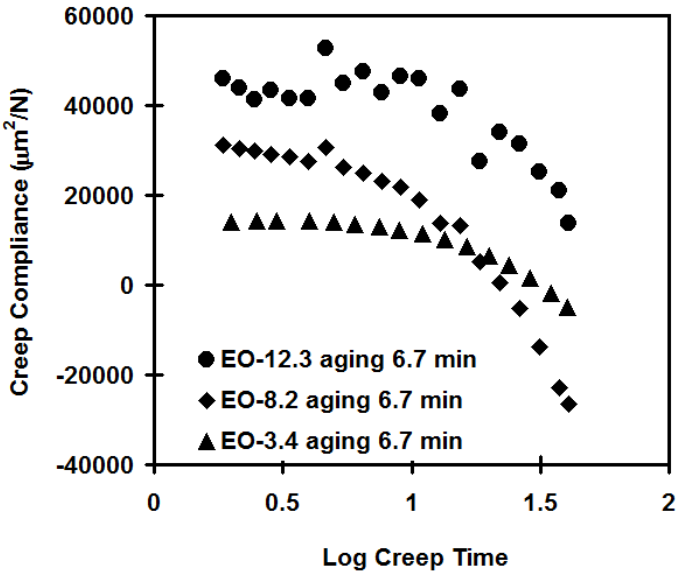

Figure 4.28. Creep study of EO-copolymers after 6.7 minutes aging.

On the other hand, for long aging times (1 hour, 3 hours, or 9 hours), the rate of increase in crystallinity (increase in the number or size of small crystals and increase in crystal perfection) is lower than at short times. This observation is consistent with the result that the creep compliance changes slowly during the creep test for long aging times. The slight increase in creep compliance with creep time at long aging time is still the largest for EO-8.2 (Figure 4.23), suggesting that the availability of amorphous chains to participate in some crystallization or crystal perfection process is still responsible for the change in creep behavior.

All of this means that aging of EO-copolymers above T_g is not as simple as Struik suggested. Similar to Struik's long-term tests, where aging during creep cannot be neglected, the actual creep compliances (Figures 4.17-4.19) have a different curvature than predicted. The negative curvature results from continuous crystallization and stiffening of the material during creep. The shape of the retardation spectrum changes during aging, which leads to a failure of the creep time-aging time-superposition. Thus, a master curve cannot be obtained by simply shifting the creep curve horizontally and/or vertically as Struik suggested. Our creep studies of EO-copolymers lead to the same conclusions as reached by McCrum and Read.[67, 68] We suggest that physical aging can be explained by the increase in crystallinity, which affects both the crystalline content and the intrinsic properties of the amorphous phase (increase in constraints).

Chapter 5. Conclusions and Suggested Future Work

The goal of this work was to study the origin of the time dependence of the structure and physical properties of EO-copolymers. The DSC, density, and creep results are explained based on an assumption that small and unstable crystals are formed at a low temperature ($T<T_{CO}$) during crystallization. These unstable small crystals can: 1) rapidly stabilize with time, which explains why $T_m^{low}(t_x)$ increases with crystallization time; 2) easily melt and recrystallize, which explains the multiple melting behavior; 3) serve as efficient thermo-reversible cross-links to increase the conformational constraints in the residual amorphous fraction. The crystallization-induced shrinkage explains the decrease in creep compliance at short aging times. The further crystal stabilization at long aging times explains the origin of the negative curvature observed in plot of creep compliance vs. time. Physical aging can be explained by the increase in crystallinity, which affects both the crystalline content and the intrinsic properties of the amorphous phase (increase in constraints). The increase in crystallinity may occur through different mechanisms at short and long crystallization times (new crystal formation, increase in crystal lateral dimensions and crystal perfection), which may explain the complicated evolution of the creep compliance as a function of creep time and aging time.

To confirm the assumption that the multiple melting behavior of EO-copolymers is the result of a melting-recrystallization-remelting process, DSC experiments carried out at much higher heating rates are suggested as future work. To carry out such experiments, I would suggest

using the newest rapid-scanning calorimeter: the Flash DSC produced by Mettler-Toledo.[89] The scan rates of Flash DSC are in the range of 30 K/min - 2.4 MK/min for heating with the sample size in the 10 ng - 1 μg range.

Bibliography

1. Khoury, F.; Passaglia, E., *Treatise on Solid State Chemistry*. Hannay N. ed.; Plenum Press: New York, 1976; Vol. 6.
2. H. Darrell Iler's Ph. D. thesis, 1995 Virginia Tech.
3. Barham, P. J.; Chivers, R. A.; Keller, A.; Martinezsalazar, J.; Organ, S. J., The Supercooling Dependence of the Initial Fold Length of Polyethylene Crystallized from the Melt - Unification of Melt and Solution Crystallization. *Journal of Materials Science* **1985,** 20, (5), 1625-1630.
4. Stack, G. M.; Mandelkern, L.; Voigtmartin, I. G., Changes in Crystallite Size Distribution during the Isothermal Crystallization of Linear Polyethylene. *Polymer Bulletin* **1982,** 8, (9-10), 421-428.
5. Hoffman, J. D.; Weeks, J. J., X-ray study of isothermal thickening of lamellae in bulk polyethylene at the crystallization temperature. *J. Chem. Phys.,* **1965,** 42, (12), 4301.
6. Hoffman, J.; Davis, G.; Lauritzen, J., *Treatise on Solid State Chemistry*. Hannay N. ed.; Plenum Press: New York, 1976; Vol. 3, p 497-614.
7. Alizadeh, A.; Richardson, L.; Xu, J.; McCartney, S.; Marand, H.; Cheung, Y. W.; Chum, S., Influence of structural and topological constraints on the crystallization and melting behavior of polymers. 1. Ethylene/1-octene copolymers. *Macromolecules* **1999,** 32, (19), 6221-6235.
8. Heck, B.; Hugel, T.; Iijima, M.; Strobl, G., Steps in the formation of the partially crystalline state. *Polymer* **2000,** 41, (25), 8839-8848.
9. Iijima, M.; Strobl, G., Isothermal crystallization and melting of isotactic polypropylene analyzed by time- and temperature-dependent small-angle X-ray scattering experiments. *Macromolecules* **2000,** 33, (14), 5204-5214.
10. Schmidtke, J.; Strobl, G.; ThurnAlbrecht, T., A four-state scheme for treating polymer crystallization and melting suggested by calorimetric and small angle X-ray scattering experiments on syndiotactic polypropylene. *Macromolecules* **1997,** 30, (19), 5804-5821.
11. Strobl, G., From the melt via mesomorphic and granular crystalline layers to lamellar crystallites: A major route followed in polymer crystallization? *European Physical Journal E* **2000,** 3, (2), 165-183.
12. Al-Hussein, M.; Strobl, G., The melting line, the crystallization line, and the equilibrium melting temperature of isotactic polystyrene. *Macromolecules* **2002,** 35, (5), 1672-1676.
13. Strobl, G., A thermodynamic multiphase scheme treating polymer crystallization and melting. *European Physical Journal E* **2005,** 18, (3), 295-309.
14. Strobl, G., Crystallization and melting of bulk polymers: New observations,conclusions and a thermodynamic scheme. *Prog Polym Sci* **2006,** 31, 398-442.
15. Lauritzen, J.; Hoffman, J., *J. Appl. Phys.* **1973,** 44, 4340-4352.
16. Clark, E. J.; Hoffman, J. D., Regime-III Crystallization in Polypropylene. *Macromolecules* **1984,** 17, (4), 878-885.
17. Hoffman, J. D.; Miller, R. L., Kinetics of crystallization from the melt and chain folding in polyethylene fractions revisited: Theory and experiment. *Polymer* **1997,** 38, (13), 3151-3212.
18. Armistead, J. P.; Hoffman, J. D., Direct evidence of regimes I, II, and III in linear polyethylene fractions as revealed by spherulite growth rates. *Macromolecules* **2002,** 35, (10), 3895-3913.
19. Kanig, G., Application of the Short-Time Staining for the Electron-Microscopic Investigation of the Crystallization of Polyethylene. *Colloid and Polymer Science* **1983,** 261, (4), 373-374.

20. Rastogi, S.; Hikosaka, M.; Kawabata, H.; Keller, A., Role of Mobile Phases in the Crystallization of Polyethylene .1. Metastability and Lateral Growth. *Macromolecules* **1991,** 24, (24), 6384-6391.

21. Okada, T.; Saito, H.; Inoue, T., Time-Resolved Light-Scattering-Studies on the Early Stage of Crystallization in Isotactic Polypropylene. *Macromolecules* **1992,** 25, (7), 1908-1911.

22. Schultz J., *"Polymer Materials Science",*. Prentice-Hall: Englewood Cliffs,NJ, 1974.

23. Groeninckx, G.; Reynaers, H.; Berghmans, H.; Smets, G., Morphology and Melting Behavior of Semi-crystalline Poly(ethylene-terephthalate).1.Isothermally Crystallized PET. *J. Polym. Sci. Polym. Phys. Ed.* **1980,** 18, 1311.

24. Fischer, E. W.; Fakirov, S., Structure and Properties of Polyethyleneterephthalate Crystallized by Annealing in Highly Oriented State. 1. Morphological Structure as Revealed by Small-Angle X-Ray-Scattering. *J. Mat. Sci.* **1976,** 11, 1041.

25. Fakirov, S.; Fischer, E. W.; Hoffmann, R.; Schmidt, G. F., Structure and Properties of Poly(ethylene-terephthalate) Crystallized by Annealing in Highly Oriented state. 2. Melting Behavior and Mosaic Block Structure of Crystalline Layers. *Polymer* **1977,** 18, 1121.

26. Bell, J. P.; Murayama, T., Relations between dynamic mechanical properties and melting behavior of nylon 66 and poly(ethylene terephthalate). *J. Polym. Sci. Part A-2* **1969,** 7, (6), 1059.

27. Schultz, J. M.; Scott, R. D., Temperature Dependence of Sceondary Crystallization in Linear Polyethylene. *J.Polym. Sci. A-2,* **1969,** 7, 659.

28. Wunderlich, B.; Mellilo, J., Morphology and growth of extended chain crystals of polyethylene. *Macromol. Chem.* **1968,** 118, 250.

29. Xu, J., Equilibrium Melting Temperature Determination of Semicrystalline Polymers through Nonlinear Hoffman-Weeks Extrapolation and Secondary Crystallization of Ethylene/Styrene Copolymers. **1999,** PhD thesis at Virginia Tech.

30. Alizadeh, A.; Sohn, S.; Quinn, J.; Marand, H.; Shank, L. C.; Iler, H. D., Influence of structural and topological constraints on the crystallization and melting behavior of polymers: 3. Bisphenol A polycarbonate. *Macromolecules* **2001,** 34, (12), 4066-4078.

31. Marand, H.; Alizadeh, A.; Farmer, R.; Desai, R.; Velikov, V., Influence of structural and topological constraints on the crystallization and melting behavior of polymers. 2. Poly(arylene ether ether ketone). *Macromolecules* **2000,** 33, (9), 3392-3403.

32. Marand, H.; Alizadeh, A., Polymer secondary crystallization: A universal model. *Abstracts of Papers of the American Chemical Society* **1999,** 218.

33. Verma, R. K.; Velikov, V.; Kander, R. G.; Marand, H.; Chu, B.; Hsiao, B. S., SAXS studies of lamellar level morphological changes during crystallization and melting in PEEK. *Polymer* **1996,** 37, (24), 5357-5365.

34. Marand, H.; Prasad, A., On the Observation of a New Morphology in Poly(Arylene Ether Ether Ketone) - a Further Examination of the Double Endothermic Behavior of Poly(Arylene Ether Ether Ketone). *Macromolecules* **1992,** 25, (6), 1731-1736.

35. Lovinger, A. J.; Davis, D. D., Solution Crystallization of Poly(Ether Ether Ketone). *Macromolecules* **1986,** 19, (7), 1861-1867.

36. Lovinger, A. J.; Hudson, S. D.; Davis, D. D., High-Temperature Crystallization and Morphology of Poly(Aryl Ether Ether Ketone). *Macromolecules* **1992,** 25, (6), 1752-1758.

37. Kruger, K. N.; Zachmann, H. G., Investigation of the Melting Behavior of Poly(Aryl Ether Ketones) by

Simultaneous Measurements of Saxs and Waxs Employing Synchrotron-Radiation. *Macromolecules* **1993,** 26, (19), 5202-5208.

38. Sohn, S.; Alizadeh, A.; Marand, H., On the multiple melting behavior of bisphenol-A polycarbonate. *Polymer* **2000,** 41, (25), 8879-8886.

39. Minakov, A. A.; Mordvintsev, D. A.; Schick, C., Melting and reorganization of poly(ethylene terephthalate) on fast heating (1000 K/s). *Polymer* **2004,** 45, (11), 3755-3763.

40. Minakov, A. M., J.; Hashimoto, T.; Huth, H.; Schick, C., , Temperature distribution in a thin-film chip utilized for advanced nanocalorimetry. *Measurement Science & Technology* **2006,** 17, (1), 199-207.

41. Papageorgiou, G. Z.; Achilias, D. S.; Bikiaris, D. N., Crystallization kinetics of biodegradable poly(butylene succinate) under isothermal and non-isothermal conditions. *Macromolecular Chemistry and Physics* **2007,** 208, (12), 1250-1264.

42. Efremov, M. Y.; Olson, E. A.; Zhang, M.; Lai, S. L.; Schiettekatte, F.; Zhang, Z. S.; Allen, L. H., Thin-film differential scanning nanocalorimetry: heat capacity analysis. *Thermochimica Acta* **2004,** 412, (1-2), 13-23.

43. Efremov, M. Y.; Olson, E. A.; Zhang, M.; Schiettekatte, F.; Zhang, A.; Allen, L. H., Ultrasensitive,fast,thin-film differential scanning calorimeter. *Review of Scientific Instruments* **2004,** 75, 179-191.

44. Zhuravlev, E.; Schick, C., Fast scanning power compensated differential scanning nano-calorimeter: 1. The device. *Thermochimica Acta* **2010,** 505, (1-2), 1-13.

45. Zhuravlev, E.; Schick, C., Fast scanning power compensated differential scanning nano-calorimeter: 2. Heat capacity analysis. *Thermochimica Acta* **2010,** 505, (1-2), 14-21.

46. Minakov, A. A.; Schick, C., Ultrafast thermal processing and nanocalorimetry at heating and cooling rates up to 1 MK/s. *Review of Scientific Instruments* **2007,** 78, (7), -.

47. Minakov, A. A.; Mordvintsev, D. A.; Tol, R.; Schick, C., Melting and reorganization of the crystalline fraction and relaxation of the rigid amorphous fraction of isotactic polystyrene on fast heating (30,000 K/min). *Thermochimica Acta* **2006,** 442, (1-2), 25-30.

48. Flory, P. J., Thermodynamics of crystallization in high polymers. IV. A theory of crystalline states and fusion in polymers, copolymers, and their mixtures with diluents. *J. Chem. Phys.* **1949,** 17, (3), 223.

49. Flory, P.; Mandelkern, L.; Hall, H., Crystallization in high polymers. VII. Heat of fusion of poly-(N,N'-sebacoylpiperazine) and its interaction with diluents. *J. Am. Chem. Soc.* **1951,** 73, 2532-2538.

50. Flory, P. J., Theory of crystallization in copolymers. *Transactions of the Faraday Society* **1955,** 51, 848-57.

51. Flory, P.; Evans, R.; Mighton, H., *J. Am. Chem. Soc.* **1950,** 72, 2018-2528.

52. Alamo, R.; Domszy, R.; Mandelkern, L., Thermodynamic and Structural-Properties of Copolymers of Ethylene. *Journal of Physical Chemistry* **1984,** 88, (26), 6587-6595.

53. Peeters, M.; Goderis, B.; Vonk, C.; Reynaers, H.; Mathot, V., Morphology of homogeneous copolymers of ethene and 1-octene .1. Influence of thermal history on morphology. *Journal of Polymer Science Part B-Polymer Physics* **1997,** 35, (16), 2689-2713.

54. Chum, P. S.; Kruper, W. J.; Guest, M. J., Materials properties derived from INSITE metallocene catalysts. *Advanced Materials* **2000,** 12, (23), 1759-1767.

55. Bensason, S.; Minick, J.; Moet, A.; Chum, S.; Hiltner, A.; Baer, E., Classification of homogeneous ethylene-octene copolymers based on comonomer content. *Journal of Polymer Science Part B-Polymer Physics* **1996,** 34, (7), 1301-1315.

56. Struik, L., *Physical ageing in amorphous polymers and other materials*. Elsevier: Amsterdam, 1978.

57. Hutchinson, J., Physical Aging of Polymers. *Prog Polym Sci* **1995,** 20, (4), 703.
58. Greiner, R.; Schwarzl, F. R., Volume Relaxation and Physical Aging of Amorphous Polymers .1. Theory of Volume Relaxation after Single Temperature Jumps. *Colloid and Polymer Science* **1989,** 267, (1), 39-47.
59. Slobodian, P.; Riha, P.; Rychwalski, R. W.; Emri, I.; Saha, P.; Kubat, J., The relation between relaxed enthalpy and volume during physical aging of amorphous polymers and selenium. *European Polymer Journal* **2006,** 42, (10), 2824-2837.
60. Kovacs, A. J., Fortsch. *Hochpolymer Forschung* **1963,** 3, 394.
61. Struik, L. C. E., The long-term physical ageing of polypropylene at room temperature. *Plastics and Rubber Processing and Applications* **1982,** 2, (1), 41.
62. Struik, L. C. E., Mechanical behaviour and physical ageing of semi-crystalline polymers:1. *Polymer* **1987,** 28, 1521.
63. Struik, L. C. E., Mechanical behaviour and physical ageing of semi-crystalline polymers:2. *Polymer* **1987,** 28, 1534.
64. Struik, L. C. E., Mechanical behaviour and physical ageing of semi-crystalline polymers:3. Prediction of long term creep from short time tests. *Polymer* **1989,** 30, 799.
65. Struik, L. C. E., Mechanical behaviour and physical ageing of semi-crystalline polymers:4. *Polymer* **1989,** 30, 815.
66. Struik L. C. E., *"Physical Aging", in "Encyclopedia of Polymer Science and Engineering"*. Wiley: New York, 2nd ed., vol. 1, 1984-1990; p 595.
67. Chai, C. K.; Mccrum, N. G., Mechanism of Physical Aging in Crystalline Polymers. *Polymer* **1980,** 21, (6), 706-712.
68. Read, B. E., Effects of physical ageing on creep in polypropylene. *Polymer* **1988,** 29, 2159.
69. Hellinckx, S., A Quantitative Model Describing Physical Aging in Isotactic Polypropylenes. *Colloid and Polymer Science* **1995,** 273, (2), 130-137.
70. Marand, H., private communication.
71. Prabhu, V.; Marand, H., unpublished results.
72. Hodge, I. M., Effects of Annealing and Prior History on Enthalpy Relaxation in Glassy-Polymers .6. Adam-Gibbs Formulation of Nonlinearity. *Macromolecules* **1987,** 20, (11), 2897-2908.
73. Hodge, I. M.; Berens, A. R., Effects of Annealing and Prior History on Enthalpy Relaxation in Glassy-Polymers .5. Mathematical-Modeling of Nonthermal Preaging Perturbations. *Macromolecules* **1985,** 18, (10), 1980-1984.
74. Hodge, I. M., Effects of Annealing and Prior History on Enthalpy Relaxation in Glassy-Polymers .4. Comparison of 5 Polymers. *Macromolecules* **1983,** 16, (6), 898-902.
75. Hodge, I. M.; Huvard, G. S., Effects of Annealing and Prior History on Enthalpy Relaxation in Glassy-Polymers .3. Experimental and Modeling Studies of Polystyrene. *Macromolecules* **1983,** 16, (3), 371-375.
76. Berens, A. R.; Hodge, I. M., Effects of Annealing and Prior History on Enthalpy Relaxation in Glassy-Polymers .1. Experimental-Study on Polyvinyl-Chloride). *Macromolecules* **1982,** 15, (3), 756-761.
77. Hodge, I. M.; Berens, A. R., Effects of Annealing and Prior History on Enthalpy Relaxation in Glassy-Polymers .2. Mathematical-Modeling. *Macromolecules* **1982,** 15, (3), 762-770.
78. Hodge, I. M., Enthalpy Relaxation and Recovery in Amorphous Materials. *Journal of Non-Crystalline Solids* **1994,** 169, (3), 211-266.

79. Unpublished result from Marand's group.
80. Tso, C. C.; DesLauriers, P. J., Comparison of methods for characterizing comonomer composition in ethylene 1-olefin copolymers: 3D-TREF vs. SEC-FTIR. *Polymer* **2004,** 45, (8), 2657-2663.
81. Gabriel, C.; Lilge, D., Comparison of different methods for the investigation of the short-chain branching distribution of LLDPE. *Polymer* **2001,** 42, (1), 297-303.
82. Zhang, M. Q.; Lynch, D. T.; Wanke, S. E., Characterization of commercial linear low-density polyethylene by TREF-DSC and TREF-SEC cross-fractionation. *Journal of Applied Polymer Science* **2000,** 75, (7), 960-967.
83. Wunderlich, B., Macromolecular physics in: crystal melting. **1980,** Vol. 3, New York, Academic Press.
84. Doak, K. W., Encycl. Polym. Sci. Eng. , 2nd edn., Wiley Interscience, 2nd edn. **1986,** vol 6, 383.
85. Kissin, Y. V., Kirk-Othmer Encycl. Chem. Technol. , Vol. 17, 4th edn., Wiley Interscience. **1996**, 702.
86. Alger, M., Polymer Science Dictionary, 2nd edn. *Chapman and Hall, 2nd edn.* **1997**.
87. Alfonso, G. C.; Pedemonte, E.; Ponzetti, L., Mechanism of Densification and Crystal Perfection of Poly(Ethylene-Terephthalate). *Polymer* **1979,** 20, (1), 104-112.
88. VanderHart, D. L.; Snyder, C. R., Proton NMR characterization of room-temperature aging after modest thermal cycling in isotactic polypropylenes. *Macromolecules* **2003,** 36, (13), 4813-4826.
89. See the website of Mettler-toledo: www.mt.com.